Journal of Structural Geology 90 (2016) 27–47

Contents lists available at ScienceDirect

Journal of Structural Geology

journal homepage: www.elsevier.com/locate/jsg

Sequential growth of deformation bands in carbonate grainstones in the hangingwall of an active growth fault: Implications for deformation mechanisms in different tectonic regimes

Atle Rotevatn [a, *], Elin Thorsheim [a, 1], Eivind Bastesen [b], Heidi S.S. Fossmark [a, 1], Anita Torabi [b], Gunnar Sælen [a]

[a] Department of Earth Science, University of Bergen, PO Box 7800, 5020 Bergen, Norway
[b] Uni Research CIPR, Allégaten 41, 5008 Bergen, Norway

ARTICLE INFO

Article history:
Received 1 February 2016
Received in revised form
30 June 2016
Accepted 14 July 2016
Available online 16 July 2016

Keywords:
Deformation bands
Damage zone
Carbonate grainstone
Compaction band
Shear band

ABSTRACT

Deformation bands in porous sandstones have been extensively studied for four decades, whereas comparatively less is known about deformation bands in porous carbonate rocks, particularly in extensional settings. Here, we investigate porous grainstones of the Globigerina Limestone Formation in Malta, which contain several types of deformation bands in the hangingwall of the Maghlaq Fault: (i) bed-parallel pure compaction bands (PCB); (ii) pressure solution-dominated compactive shear bands (SCSB) and iii) cataclasis-dominated compactive shear bands (CCSB). Geometric and kinematic analyses show that the bands formed sequentially in the hangingwall of the evolving Maghlaq growth fault. PCBs formed first due to fault-controlled subsidence and vertical loading; a (semi-)tectonic control on PCB formation is thus documented for the first time in an extensional setting. Pressure solution (dominating SCSBs) and cataclasis (dominating CCSBs) appear to have operated separately, and not in concert. Our findings therefore suggest that, in some carbonate rocks, cataclasis within deformation bands may develop irrespective of whether pressure solution processes are involved. We suggest this may be related to stress state, and that whereas pressure solution is a significant facilitator of grain size reduction in contractional settings, grain size reduction within deformation bands in extensional settings is less dependent on pressure solution processes.

1. Introduction

Deformation bands are tabular, mm-wide zones of localized shear and/or volume loss/gain that form in porous granular rocks through grain reorganization (disaggregation), grain crushing (cataclasis) and/or dissolution/precipitation (pressure solution, cementation) processes. Deformation bands have been mainly known to form in high-porous sandstones; natural examples are widely reported in the geological literature since the late 1970s (e.g. Aydin, 1978; Aydin and Johnson, 1978, 1983; Antonellini et al., 1994; Fossen and Hesthammer, 1997), and has later been supplemented by studies focusing on emulating deformation band growth through laboratory experiments (e.g. Mair et al., 2000; Mair et al., 2002; Vajdova et al., 2004) as well as in numerical models (e.g. Antonellini and Pollard, 1995; Klimczak et al., 2011; Chemenda et al., 2012). It is also well-established that deformation bands in porous sandstones may be associated with a bulk reduction in permeability in the range of 1–3 (occasionally up to six) orders of magnitude relative to host rock (e.g. Antonellini and Aydin, 1994; Taylor and Pollard, 2000; Sternlof et al., 2004; Fossen et al., 2007; Rotevatn et al., 2008; Ballas et al., 2012; Rotevatn et al. 2013); for pure compaction bands (sensu Mollema and Antonellini, 1996) in porous sandstones, up to 3 magnitude order permeability reductions have been reported (Baud et al., 2012; Deng et al., 2015).

Deformation bands in porous carbonate rocks, on the other hand, were first reported from laboratory experiments (Baud et al., 2000; Vajdova et al., 2004). Natural examples of these bands have been reported since the mid-2000s (Marchegiani et al., 2006; Micarelli et al., 2006; Tondi et al., 2006). Further studies have followed, including experimental work (Baxevanis et al., 2006; Baud et al., 2009; Vajdova et al., 2010; Zhu et al., 2010; Cilona et al., 2012, 2014; Ji et al., 2015) and field-based studies that document deformation bands predominantly in carbonate grainstones

* Corresponding author.
E-mail address: atle.rotevatn@uib.no (A. Rotevatn).
[1] Now at: Statoil, Sandslivegen 90, 5254 Sandsli, Norway.

http://dx.doi.org/10.1016/j.jsg.2016.07.003

(Antonellini et al., 2008; Agosta et al., 2009; Cilona et al., 2012; Rustichelli et al., 2012; Tondi et al., 2012; Antonellini et al., 2014b), and recently also in chalk (Wennberg et al., 2013).

In general, deformation bands in carbonate rocks exhibit many similarities to their sandstone counterparts. This includes (i) that they are characterized by localized grain-scale shear in a mm-to-cm-scale zone rather than along a discrete slip surface (e.g. Tondi et al., 2006), (ii) strain hardening behaviour (Baud et al., 2009; Cilona et al., 2012; Ji et al., 2015), (iii) scaling properties (Tondi et al., 2012), (iv) magnitude of displacement (e.g. Tondi et al., 2006; Antonellini et al., 2008), (v) failure modes (Vajdova et al., 2004; Baxevanis et al., 2006; Cilona et al., 2014), (vi) sensitivity to changes in porosity and the shape and size of grains (Rustichelli et al., 2012; Cilona et al., 2014), and (vii) porosity-permeability reduction (Rath et al., 2011; Antonellini et al., 2014a; Tondi et al., 2016). However, there are other aspects of carbonate deformation bands that make them different from deformation bands in porous sandstones. *First*, whereas grain reorganization and cataclasis are the chief mechanisms for accommodating shear and compaction in porous sandstones (e.g. Antonellini et al., 1994; Fossen et al., 2007), pressure solution (in concert with cataclasis) seems to play a far more significant role in compaction- and shear localization in carbonate rocks, and appear to commonly occur at near-surface burial depths (e.g. Tondi et al., 2006, 2012; Cilona et al., 2012; Cilona et al., 2014). In fact, intergranular pressure solution is an important process that contributes to grain size and porosity reduction in deformation bands in grainstones (e.g. Tondi et al., 2006; Tondi, 2007; Rustichelli et al., 2012). However, there are also studies that report non-cataclastic and cataclastic deformation bands in porous carbonate rocks where evidence for pressure-solution processes is absent (Rath et al., 2011). Furthermore, Antonellini et al. (2014b) highlight a different micro-mechanism of deformation in carbonate rocks composed of soft micrite peloids, namely soft plastic deformation and subsequent smearing of the peloids, where grain crushing and pressure solution are subordinate micro-mechanisms. This plastic smearing is interpreted by Antonellini et al. (2014b) to occur due to the intragranular microporosity present in the peloids. *Second*, cataclasis, as a mechanism for strain accommodation in carbonate deformation bands, appears to be widespread at shallow burial depths (e.g. Micarelli et al., 2006; Tondi et al., 2012, 2016; Antonellini et al., 2014a). Contrastingly, in natural deformation bands in porous sandstones at shallow burial depths, grain reorganization is common (Mandl et al., 1977; Du Bernard et al., 2002; Bense et al., 2003); grain crushing in shallowly buried, poorly-consolidated sandstones have been reported in some cases (Cashman and Cashman, 2000; Rawling and Goodwin, 2003; Balsamo and Storti, 2011; Alikarami and Torabi, 2015) but is generally considered to be more common at greater burial depths (Mair et al., 2002; Fossen et al., 2007).

Third, and as a consequence of the former two points, permeability heterogeneity forming at shallow burial depths is more of a concern in carbonate rocks than in sandstones; deformation bands dominated by pressure solution and cataclasis, which may form at near-surface burial depths in porous carbonate rocks, may reduce permeability by 1–4 orders of magnitude (Rath et al., 2011; Antonellini et al., 2014a; Tondi et al., 2016). In poorly consolidated sandstones at shallow burial on the other hand, deformation is dominated by non-cataclastic bands that generally have little influence on permeability (Fisher and Knipe, 2001; Fossen et al., 2007). Rath et al. (2011) suggest that the reason for this difference may be that carbonates are able to accommodate strain by crystal plastic deformation (e.g. twinning, solution, and precipitation) already at shallow burial depths, in contrast to siliciclastic sediments where this is generally not possible.

Despite the significant progress made by previous workers, significantly less is known about the deformation bands in carbonate rocks compared to those of porous sandstones. Furthermore, the majority of existing studies of natural deformation bands in carbonate rocks clusters around a relatively small number of study areas predominantly in Italy (Table 1 and references therein). More outcrop studies are therefore needed in order to gain further insight to the structure, kinematics, and deformation mechanisms of deformation bands in carbonate rocks. This is particularly the case for extensional tectonic settings, since most previous studies have focused on contractional tectonic settings (Table 1).

The present study focuses on the structure and evolution of deformation bands in carbonate grainstones within syn-rift carbonate grainstones of the Globigerina Limestone Formation in Malta (Fig. 1), and we document for the first time the sequential development of compaction bands and compactive shear bands in the hangingwall of an extensional growth fault. In doing so, we aim to contribute towards improving the general understanding of the structure and evolution of deformation bands in porous carbonate rocks. This key aim is addressed through the following set of specific objectives; (i) to document and describe the geometry, morphology, microstructure and kinematics of the studied deformation bands; (ii) determine their porosity; (iii) elucidate their spatiotemporal evolution; (iv) discuss their mechanisms and conditions for formation, in light of previously published work.

Table 1
Overview of field areas where natural deformation bands in carbonate rocks have been studied.

Country	Region	Field location	References	Tectonic setting
Italy	Central Appenines	Majella Mountain	Marchegiani et al., 2006; Tondi et al., 2006; Antonellini et al., 2008; Agosta et al., 2009; Cilona et al., 2012; Cilona et al., 2014; Rustichelli et al., 2012; Tondi et al., 2016.	Contraction
	Northern Appenines	Cingoli Anticline	Antonellini et al., 2014b	Contraction
	NW Sicily	Favignana Island	Tondi et al., 2012; Tondi et al., 2016.	Contraction
		San Vito lo Capo peninsula	Tondi, 2007; Antonellini et al., 2014a	Contraction
	SE Sicily	Hyblean Plateau	Micarelli et al., 2006	Extension (syn-contractional)
Norway	Southern North Sea	Oseberg field	Wennberg et al., 2013	Extension
Austria/ Hungary	Austrian-Hungarian border	Eisenstadt-Sopron sub-basin of the Vienna Basin	Rath et al., 2011	Extension (subsequently also transtension and inversion)

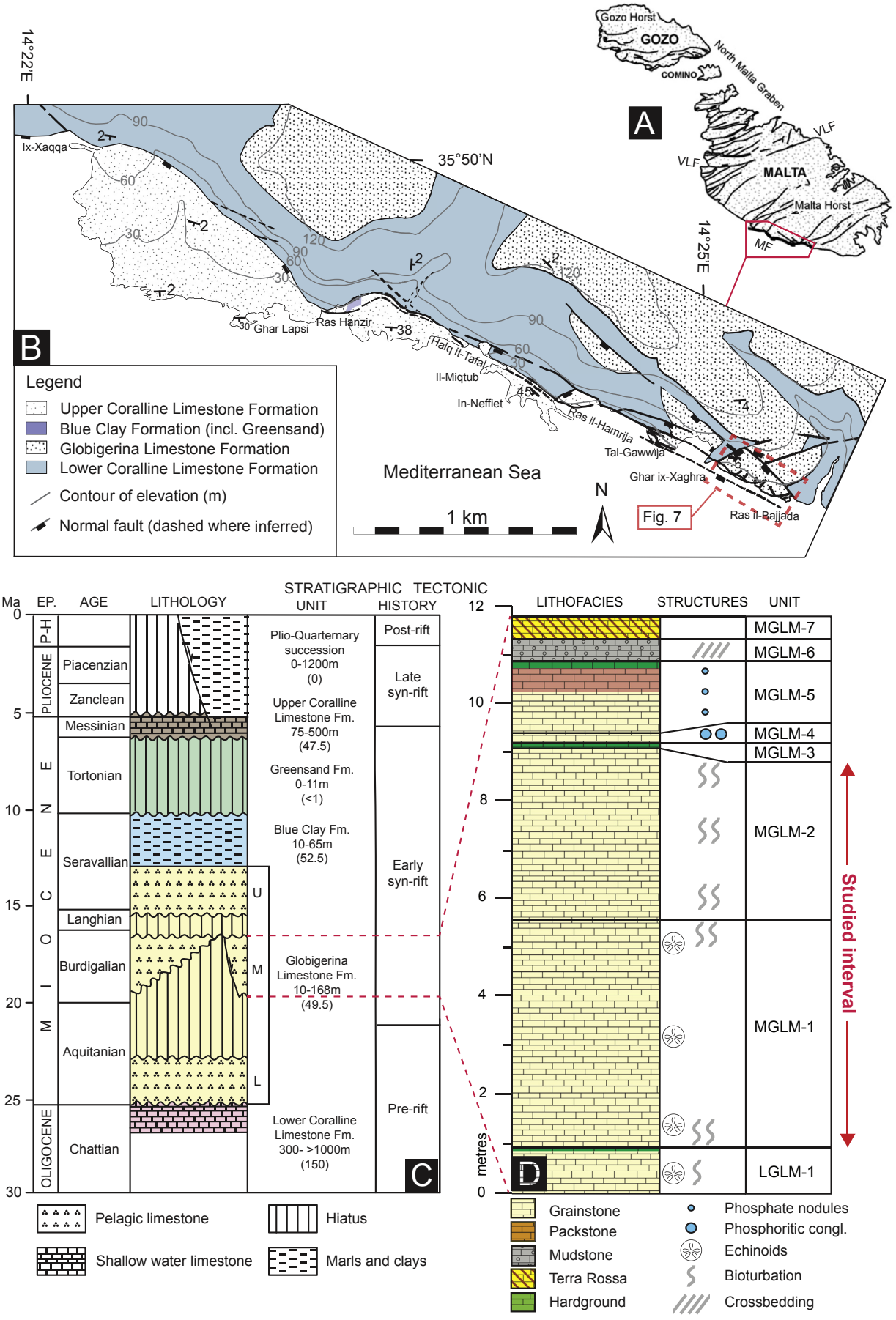

Fig. 1. (A) Map showing the location of major normal faults in Malta. MF = Maghlaq Fault; VLF = Victoria Lines Fault. Based on Dart et al. (1993) and Bonson et al. (2007). (B) Geological map of the Maghlaq Fault, outcropping along 4 km of the southwestern coastline of Malta. Note that individual members of the stratigraphic formations are not distinguished on the map. The topographic contour intervals are in meters above sea level. Location is shown in (A). The study area is located in the ESE, marked by the red polygon and shown in Fig. 7. Based on Dart et al. (1993) and Bonson et al. (2007). (C) Tectono-stratigraphic log of the Oligocene-Quaternary age sediments of the Maltese archipelago. EP = epoch; P-H = Pleistocene-Holocene. Stratigraphic thickness ranges are based on Pedley (1993) and Bonson et al. (2007) and are from onshore Malta, whereas values in brackets indicate local thicknesses along the Maghlaq Fault. (D) Schematic sedimentary log of the stratigraphy in the study area. LGLM = Lower Globigerina Limestone Member; MGLM = Middle Globigerina Limestone Member. (For interpretation of the references to colour in this figure legend, the reader is referred to the web version of this article.)

2. Regional tectonic and stratigraphic framework

Malta is located on the NE shoulder of the Pantelleria rift system within the Pelagian block, which represents the northernmost part of the African continental plate (Dart et al., 1993; their Fig. 1). The WNW-trending Pantelleria Rift (or Sicily Channel Rift Zone) is c. 100 km wide and 600 km long (Grasso et al., 1986) and developed from late Oligocene times until Messinian times (Cello et al., 1985). The Pantelleria Rift developed in response to extension localizing in the central part of the Pelagian block, between Tunisia and Sicily, likely driven by back-arc N-S-directed extension related to Apennine-Maghrebian shortening (Argnani, 1990). Despite its location on the rift shoulder, the only major fault onshore Malta with a Pantelleria rift trend is the studied Maghlaq Fault (Bonson et al., 2007, Fig. 1). The ENE-WSW trending North Malta Graben and North Gozo Graben (and the intervening Malta and Gozo Horsts) dissect the WNW-orientated Pantelleria rift trend at acute angles of 32° and 66°, respectively, and constitute the main structural grain on the islands. These fault trends are considered to be coeval with the Pantelleria rift, having formed under the same, N-S directed extension (Dart et al., 1993), consistent with Argnani (1990). Uplift of the northern rift flank of the Pantelleria rift, combined with a falling sea-level, caused the emergence of the Maltese archipelago during early Messinian times (Bonson et al., 2007).

The stratigraphy of the Maltese islands (Fig. 1) can be subdivided with respect to the Pantelleria rifting event (Pedley et al., 1976; Dart et al., 1993; Bonson et al., 2007) into pre-rift (>21 Ma), early syn-rift (21-6 Ma), late syn-rift (<6–1.5 Ma) and post-rift deposits (probably <1.5 Ma); (i) the pre-rift strata consist of Lower Coralline Limestone Formation platform carbonates and Lower Globigerina Limestone Member pelagic carbonates; (ii) the early syn-rift strata consists of the Middle to Upper Globigerina Limestone Member (the Middle Globigerina Limestone Member being the interval of interest in this study), as well as the Blue Clay and Greensand Formations, and the lowermost part of the Upper Coralline Limestone Formation; (iii) the late syn-rift strata is comprised of platform and slope carbonates of the Upper Coralline Limestone and a Plio-Quaternary succession of marls and carbonate mudstones; (iv) the post-rift succession comprises Quaternary to recent hemipelagic and turbiditic muds offshore, and Quaternary talus and alluvial fan deposits onshore.

3. Structure and stratigraphy of the study area

The Maghlaq Fault (MF), located on the southern coast of Malta (Figs. 1 and 2), is a SSW-facing, left-stepping, en-echelon normal fault array comprised of relatively straight, 1–2 km long, WNW-ESE trending fault segments linked by shorter (50–400 m long) E-to ENE-trending segments (Bonson et al., 2007). The study area is located in the hangingwall of a segment of the ESE-most part of the exposed MF, at Ras il-Bajjada (Figs. 1 and 2). Here, the Lower Coralline Limestone Formation and the Lower Globigerina Limestone Member in the footwall are juxtaposed against the Lower to Middle Globigerina Limestone Member in the hangingwall, suggesting a throw in the range of 50–80 m. The focus of this study are deformation bands that are distributed throughout the MF hangingwall within the early syn-rift Middle Globigerina Limestone Member (MGLM; see Fig. 2); Bonson et al. (2007) first reported these bands, but they have not previously been studied in detail. The MGLM is outcropping in a belt of wavecut platforms and cliff sections over an area approximately 350 m long and 20–30 m wide along the coastline. The study area is affected by approximately 10 subsidiary normal faults (throw <3 m) with an ENE-WSW to NE-SW trend, which we will henceforth refer to as 'intrablock faults'. The Maghlaq Fault segment in the study area exhibit pure dip-slip normal-sense displacement; the intrablock faults are associated with slightly oblique but predominantly dip-slip normal-sense displacement. The studied part of the MGLM (Fig. 1D) is comprised of a c. 8 m thick succession of bioclastic grainstones (sensu Dunham, 1962). The upper 3.5 m of the studied grainstones are heavily bioturbated (MGLM-2 in Fig. 1D), whereas the lowermost 4.5 m are bioturbated near the top and base, but otherwise not (MGLM-1 in Fig. 1d). Other than the variable degree of bioturbation, the 8 m grainstone succession appears massive and homogeneous with little sedimentological variability. The studied grainstones are separated from the Lower Globigerina Limestone Member (LGLM-1 in Fig. 1d) at the base by a hardground, and capped at the top by another hardground (MGLM-3 in Fig. 1d) and a phosphatic conglomerate bed (MGLM-4 in Fig. 1d). The maximum burial depth of the studied interval is approximately 250 m (Bonson et al., 2007).

4. Methodology

A standard polarizing light microscope of the type Nikon Eclipse 400 POL was used to analyse the thin sections. A ZEISS Supra 55VP Field Emission Scanning Electron Microscope with a spatial resolution of 0.8 nm and magnification of $>10^9$X, was used for further analysis of the thin sections.

Porosity measurements were carried out using different laboratory and image analysis techniques. Image-based porosity analyses were performed on thin section photomicrographs and backscatter (BSE) images using the software ImageJ 1.46r (Ferreira and Rasband, 2012). Thin section photomicrographs provide a basis for estimating 2D macroporosity (porosity resolvable using optical microscope imagery) termed 'Total Optical Porosity' (TOP) herein, whereas the BSE images allows for a determination of 2D macro-*and* microporosity combined (microporosity being porosity that falls below the resolution of optical microscope imagery, but which is resolvable using BSE imagery), termed 'BSE porosity' herein. All porosity measurements are present-day porosity, or effective porosity, and thus do not include secondary cement precipitated in pores. A total of 10 thin sections were analysed, on which 83 porosity measurements were conducted on optical photomicrographs, and 24 on BSE images. Nine of the analysed thin sections contained a combination of deformation bands and surrounding host rock; one of the samples was a host rock sample with no deformation bands. Several measurements on each thin section were conducted to capture porosity variations within host rock, deformation bands, and transition zones between deformation bands and host rocks. In addition to this, six core plugs were analysed at the petrophysics laboratory at the University of Manchester, where porosity was determined using a using a ResLab DHP-100 digital helium porosimeter. The core plugs have a diameter of one inch and range in length from 5.8 to 7.0 cm. Of these six samples, three were host rock core plugs and three contained host rock and one single deformation band.

5. Host rock characterization

The bioclastic grainstones of the MGLM are composed predominantly of spherical planktonic foraminifers (mainly globigerinids), elongated bivalve shells and plates and spines of echinoderms (Fig. 3). The maximum size of the foraminifers and echinoderm-fragments are c. 170 μm and 300 μm, respectively. The host rock is characterized by both intergranular (Pi) and intragranular (Pii) porosity (sensu Choquette and Pray, 1970, Fig. 3), as well as intra-cement microporosity (Fig. 4). The intragranular porosity is mainly contained within the chambers of the

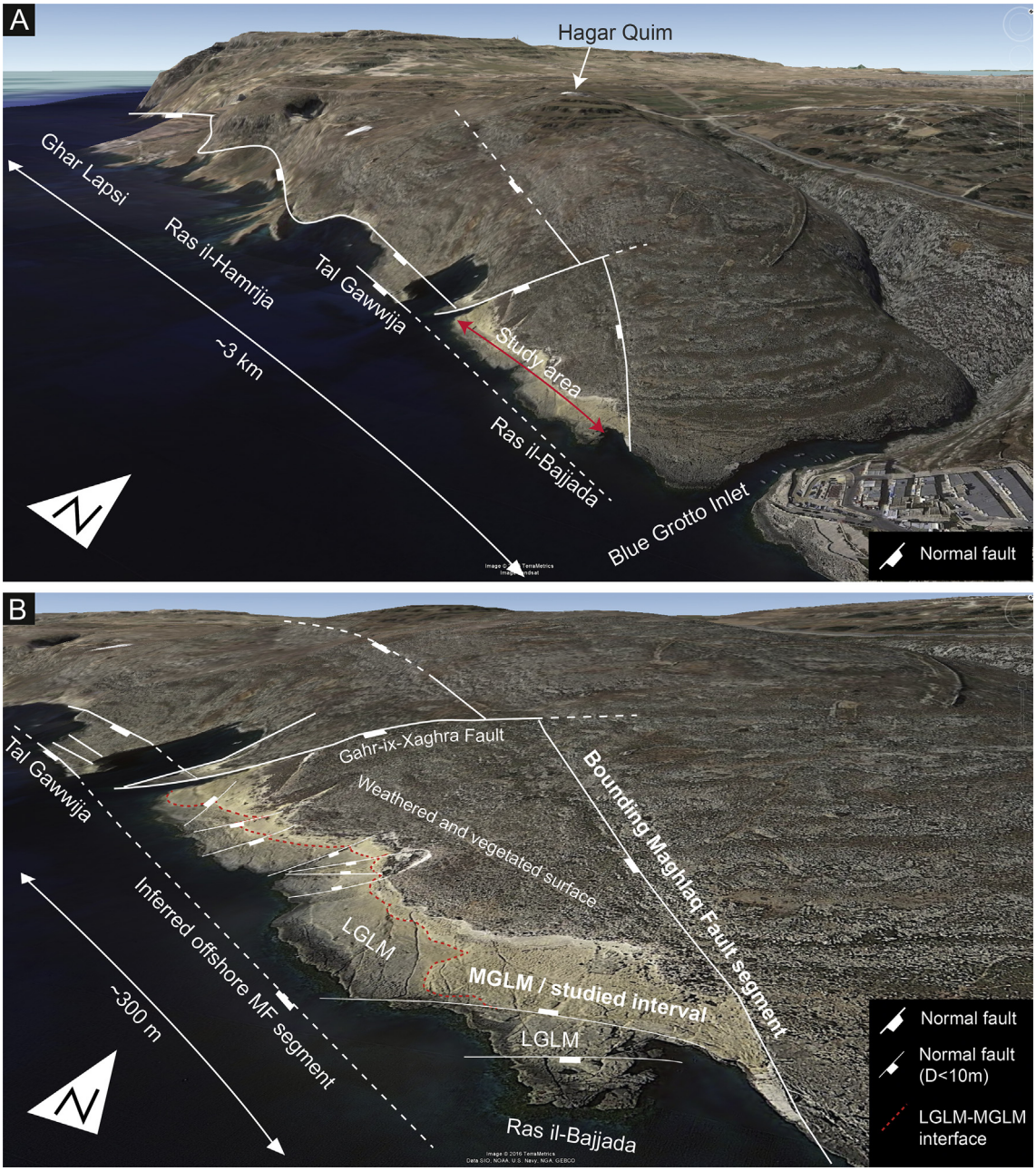

Fig. 2. Panoramic view onto satellite imagery draped on digital elevation model showing the WSW coastline of Malta, with (A) the wider Maghlaq Fault system and (B) a close-up of the study area in the ESE. The location of the study area shown in (B) is indicated in (A). The vertical scale is exaggerated by a factor of 2 in (A), whereas no vertical exaggeration is applied in (B). MF = Maghlaq Fault; LGLM = Lower Globigerina Limestone Member; MGLM = Middle Globigerina Limestone Member. Imagery courtesy of Google Earth.

foraminifers, whereas the intergranular porosity is located between individual grains. The pore sizes are generally below 100 μm and do not exceed 200 μm (long axis measured; Figs. 3 and 4). The rock is comprised predominantly of calcite, with quartz and clay minerals in accessory amounts only. Scattered clasts of quartz occur, in the size range of approximately 20–40 μm. Fine to cryptocrystalline matrix appears under the optical microscope as dark brown to black patches between grain contacts and within foraminifers (Fig. 3), and consist of small (<10 μm) carbonate fragments, clay minerals and quartz (Fig. 4A). Fractures within the grains occur, but are not abundant. The occasional fracturing is restricted to single grains (intragranular fractures) and mainly affects the echinoderm-fragments, but rarely the foraminifers (Fig. 4B and C).

Calcite cement is present in the host rock, including in the chambers of the foraminifers (Fig. 4D). Generally, three types of calcite cement can be distinguished: (i) syntaxial (Fig. 4E), (ii) blocky, and (iii) dogtooth cement (Fig. 4F). The syntaxial cement is present around plates and spines of echinoderm fragments, and typically fills the intergranular pore space adjacent to the echinoderms. Echinoderm fragments are porous and composed of single calcite crystals, and the cement grew in optical continuity with the single crystals. The dogtooth-cement displays up to 30-μm long calcite scalenohedral crystals that grow with their long-axis perpendicular or sub-perpendicular to the bioclastic substrate (Fig. 4F). This cement is commonly present in the intergranular pore space between the bioclasts, as well as in the intragranular pores of the foraminifers where it is seen coating the pore walls.

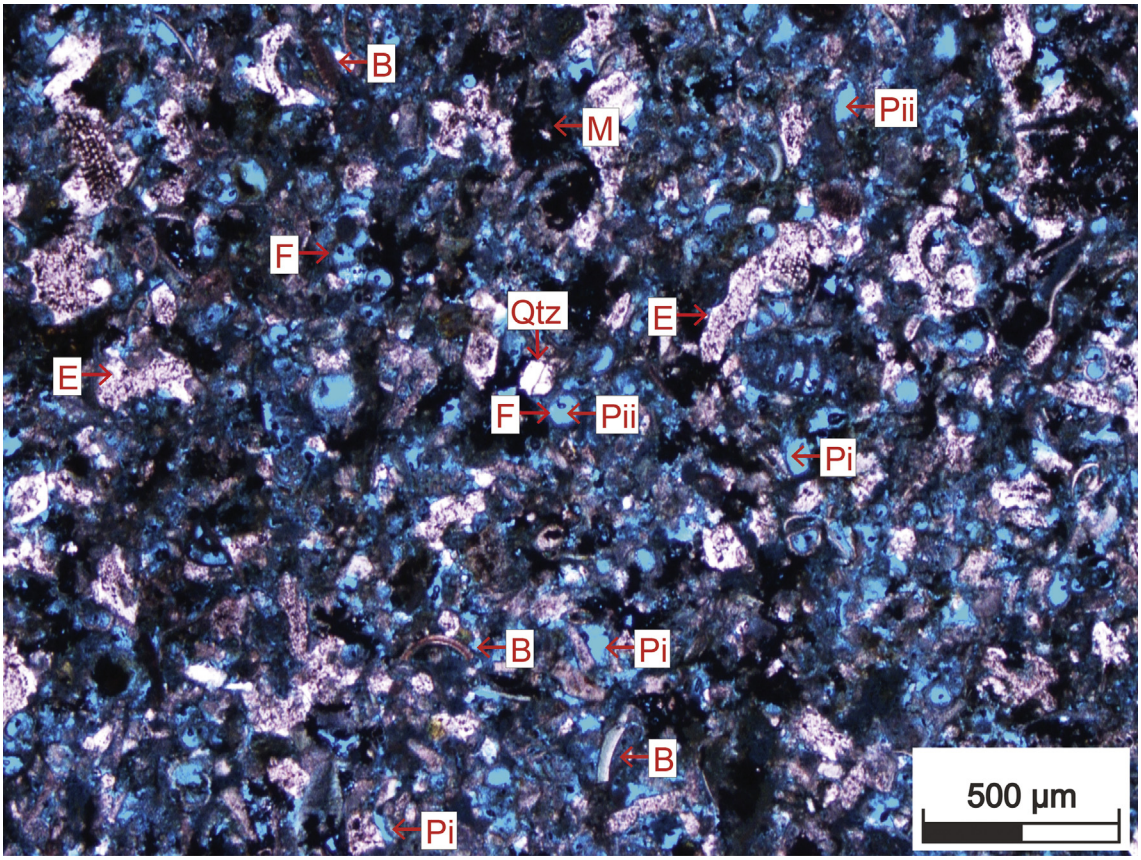

Fig. 3. Thin section photomicrograph (plane-polarized light) of the studied grainstone host rock of the Middle Globigerina Limestone Member. The samples were impregnated with epoxy prior to thin section preparation, which makes the pore space stand out in blue. The abundant echinoderm-fragments (E), bivalves (B) and foraminifers (F) are highlighted. Note the presence of intergranular (Pi) and intragranular (Pii) porosities, as well as quartz grains (Qtz) and matrix (M). (For interpretation of the references to colour in this figure legend, the reader is referred to the web version of this article.)

6. Structural analysis of the studied deformation bands

The studied deformation bands were classified (following Aydin et al., 2006) on the basis of i) orientation relative to bedding, ii) presence/absence of observable shear offset, iii) porosity contrast to host rock and iv) dominant deformation mechanism; the evidence is presented in the following. The MGLM in the hangingwall of the MF exhibits two distinctly different types of deformation bands, of which the latter has two sub-types: pure compaction bands (Type 1; PCBs), and compactive shear bands (Type 2; CSBs), of which there are solution-dominated compactive shear bands (Type 2a; SCSBs) and cataclasis-dominated compactive shear bands (Type 2b; CCSBs).

6.1. Pure compaction bands (type 1)

Structures recognized as PCBs are sub-horizontal and oriented parallel to sedimentary bedding (Fig. 5). There is no observable shear offset associated with the bed-parallel PCBs; all CSBs (Type 2a and 2b) abut against the bed-parallel PCBs (Fig. 5A). The PCBs are localized within an approximately 30 cm thick, slightly finer-grained, erosionally-recessed interval within the MGLM-2 (Fig. 1D). The bands have relatively straight and planar outcrop-scale morphology, as opposed to the 'wiggly' or 'chevron' nature of some (but not all) pure compaction bands in porous sandstones (e.g. Eichhubl et al., 2010; Fossen et al., 2015; Liu et al., 2015; Torabi et al., 2015). On the microscale, PCBs typically exhibit undulating/irregular contacts to the surrounding host rock (Fig. 6); PCB thickness is variable along strike, ranging from c. 750 to 1500 μm, whereas length of individual PCBs is in the range of 0.5–2 m. Texturally, PCBs comprise tightly packed bioclasts. Loss of pore space relative to the host rock is evident within the PCBs, and is interpreted as evidence of compaction. In the PCB depicted in Fig. 6, significantly less pore space (blue epoxy) is present within the bands compared to the surrounding host rock. High-resolution BSE images reveal evidence of sutured grain contacts in the bands (Fig. 6C). Pressure solution processes are therefore, along with mechanical grain reorganization, interpreted as being responsible for accommodating the compaction within the bands. No evidence of grain fracturing or crushing was observed in the PCBs.

6.2. Compactive shear bands (type 2)

Structures recognized as CSBs are generally orientated at high angle to bedding and are widely distributed across the study area (Figs. 5 and 7). The bands occur within the non-bioturbated part of the lowermost 4.5 m of the MGLM grainstones (MGLM-1; Fig. 1D); the bioturbated part of the succession does not host deformation bands. The CSBs are protruding, forming mm-scale relief on the outcrop surface. The CSBs have light yellow-to-light-brown colour, generally not contrasting that of the host rock (Fig. 5b) except where black-to-brown iron oxide varnish colours the weathering surface of the host rock but not the bands (Fig. 8). The bands feature a dominant ENE-trend, oblique to the local NW-trend of the Maghlaq Fault, but sub-parallel to the subsidiary intrablock faults

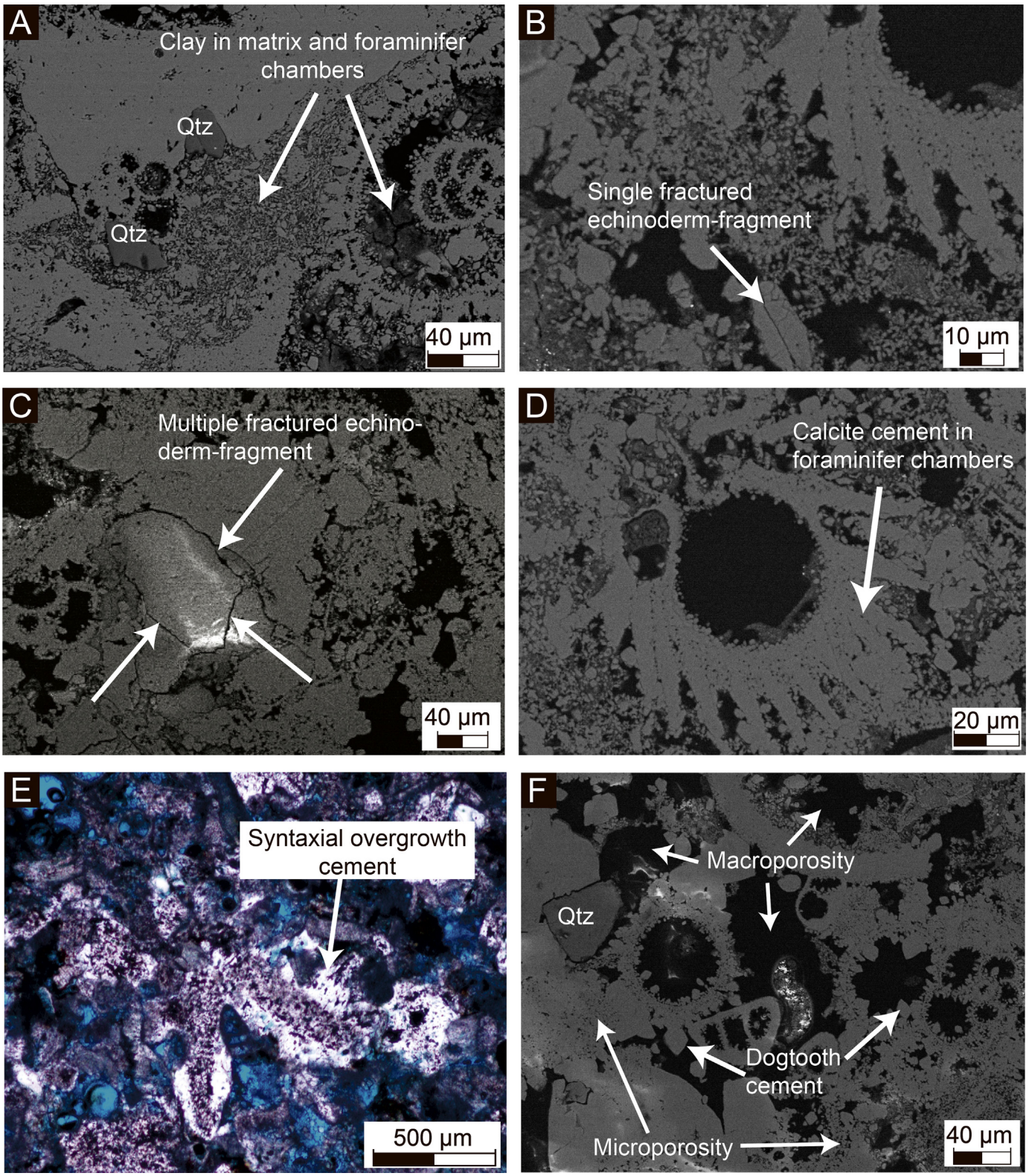

Fig. 4. BSE images and thin section photomicrograph (plane-polarized light) of the MGLM host rocks. In the greyscale BSE images (A-D and F) the pore space is black, while grains are grey. (A) Clay is present in the matrix and chambers of foraminifers. Note the scattered quartz grains (Qtz) in the sample. (B) Echinoderm fragment affected by a single fracture. (C) Echinoderm fragment affected by multiple fractures. (D) Calcite cement in chambers of foraminifers. (E) Thin section photomicrograph (plane-polarized light) of syntaxial overgrowth cement on echinoderm spines. (F) Dogtooth-cement in the host rock, where white arrows point to the blunted terminations of the calcite crystals. Note the presence of pores at various scales.

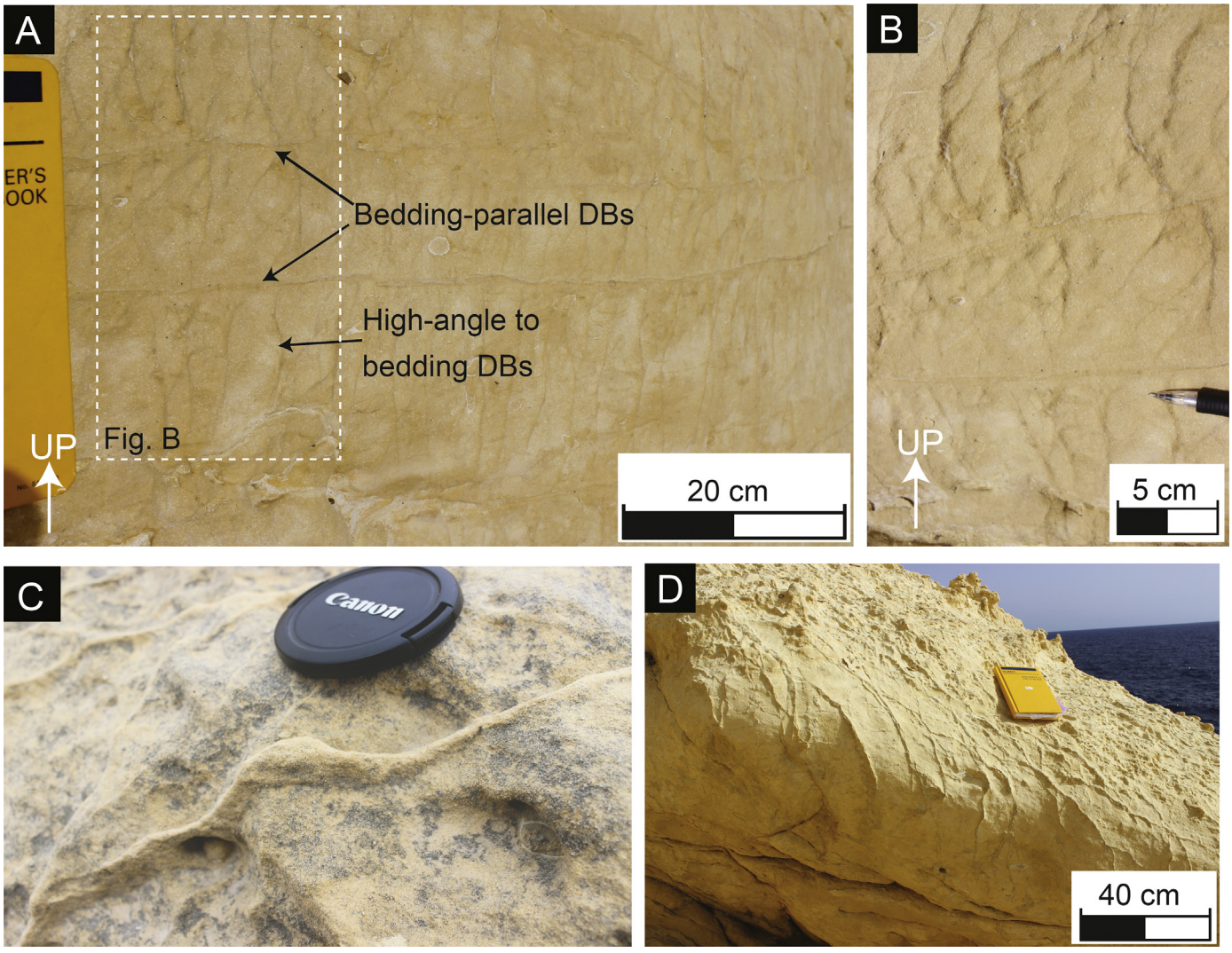

Fig. 5. Field relations of deformation bands. (A) Deformation bands at high-angle to bedding (compactive shear bands) abut against bed-parallel deformation bands (pure compaction bands) in the MGLM. (B) Close-up of the deformation bands depicted in (A); no cross-cutting relations between compactive shear bands (high angle to bedding) and pure compaction bands (bed-parallel) is observed. (C) Compactive shear bands are light-coloured, millimetre-thick structures that form protruding ridges on the surfaces studied. (D) Compactive shear bands generally exhibit a high angle to the sedimentary bedding. White arrows in (A) and (B) indicate stratigraphic way up.

(throw <3 m) in the hangingwall (Fig. 7). Direct shear-sense indicators are hard to find in the very homogeneous host rock, but where visible they indicate normal-sense shear. Their sub-parallel strike to that of the intrablock faults also support this, since the intrablock faults are also dominated by dip-slip normal-sense movement. The CSB occur in outcrop as i) single bands with thicknesses generally in the range of 1–4 mm (Fig. 8A and B), and to some extent ii) deformation bands clusters comprised of 10s of bands and that are up to 20 cm wide (Fig. 8C), but more commonly iii) anastomosing networks, or swarms, ranging from 0.5 m to 5 m in width (Fig. 8D and E). Note that although single CSBs range in thickness between 1 and 4 mm, there is significant along-strike variability within individual bands (Fig. 9A). CSB lengths are generally short (less than a few 10s of cm) as they predominantly occur in networks where they intersect (abut or cross-cut) with other bands and it is therefore generally difficult to assess their unrestricted length; where single bands occur undisturbed by other bands, however, they are up to 10 m long. CSB frequency within the studied interval is relatively high; CSB frequency at distance from faults (i.e. more than 10 m away from faults) is generally in the range of 4–6 CSBs per meter. CSB frequency shows a significant increase near faults; adjacent to the MF in the ESE part of the study area, CSB frequency peaks at c. 35 CSBs per meter. CSB frequency also rises to 10–12 CSBs per meter near the smaller intrablock faults. Although indistinguishable in outcrop, microstructural analysis reveals that whereas some of the CSBs are dominated by pressure-solution features (SCSB; Type 2a), others are dominated by cataclastic deformation (CCSB, Type 2b). We therefore provide a separate microstructural description for the two types of CSBs in the following.

6.2.1. Solution-dominated compactive shear bands (type 2a)

Structures recognized as SCSBs (Fig. 9) are oriented at high angles to the bedding, and grain reorganization within the bands is evidenced by alignment of elongated bioclasts parallel to the boundaries of the band (Fig. 9C). Clear evidence of compaction associated with the deformation bands is seen as a reduction of pore space within the bands (Figs. 9 and 10). In the SCSB depicted in Fig. 9, the porosity (TOP) is reduced to 6.7%, relative to the host rock with a porosity of 13.3%.

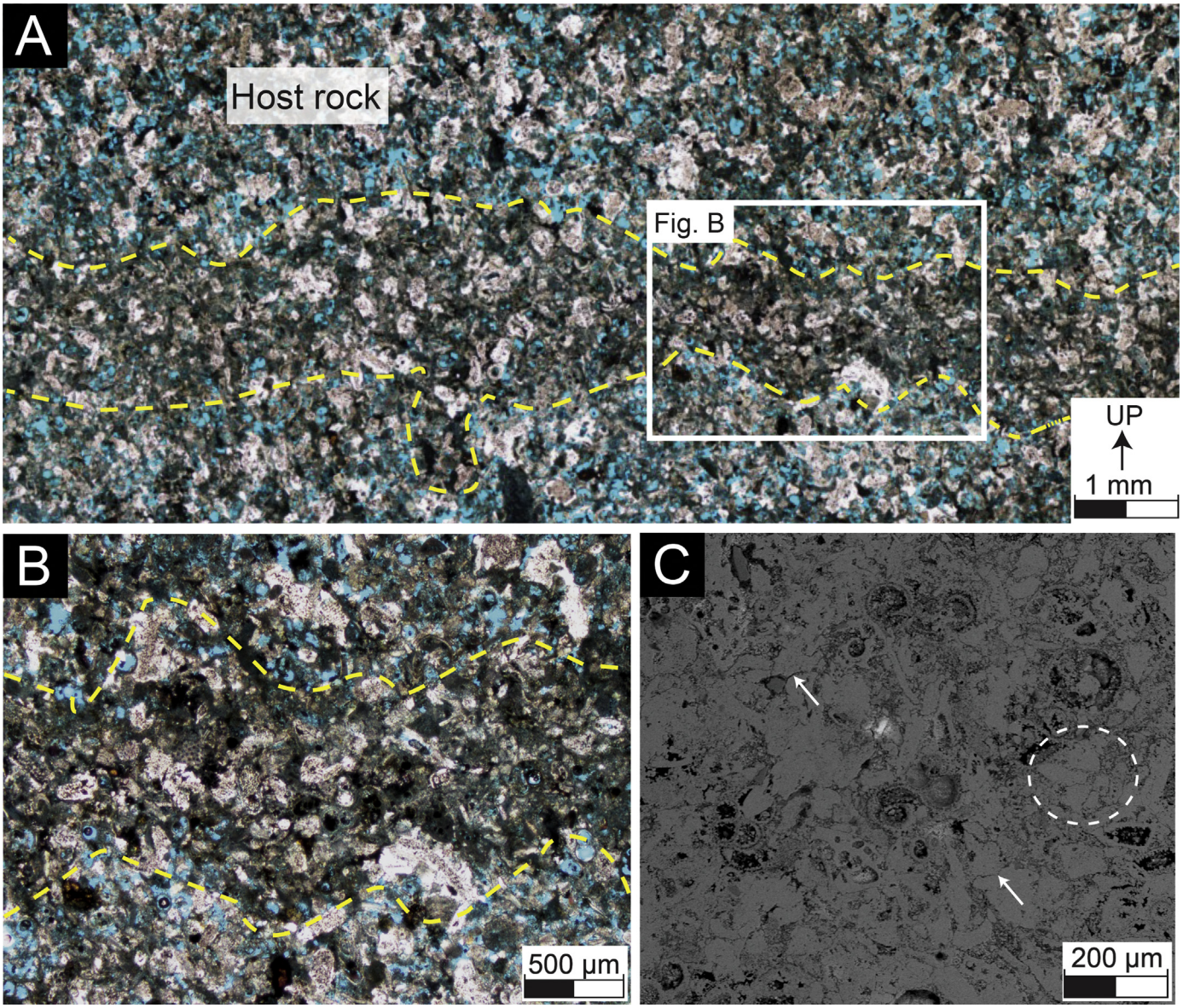

Fig. 6. Pure compaction band (Type 1) imagery. (A) Thin section photomicrograph (plane-polarized light) of a pure compaction band (Type 1) oriented parallel to the sedimentary bedding in the MGLM. Note the black arrow indicating stratigraphic way up. The boundary of the band delineates the low-porosity zone represented by the band; note the lesser porosity (blue epoxy) within the band. (B) Close-up of the same pure compaction band; location of the close-up is shown in (A). The band has irregular contacts to the surrounding host rock and the porosity (blue) in the band is significantly reduced, relative to the more porous host rock. No evidence of shear deformation or cataclasis is observed in the bed-parallel pure compaction bands. (C) BSE image inside a pure compaction bands. The white arrows indicate sutured grain contacts, indicative of pressure solution having operated at grain contacts between the bioclasts in the band. The dashed circle highlights an area with several grains with sutured grain contacts. (For interpretation of the references to colour in this figure legend, the reader is referred to the web version of this article.)

SCSBs are typically comprised of a central zone separated from the surrounding host rock by a transition zone (Fig. 10); this is similar to band architectures reported in porous carbonates (Tondi et al., 2006) and sandstones (Antonellini and Aydin, 1994; Alikarami and Torabi, 2015). The transition zone is not visible at outcrop scale. The transition zones have a less tight grain packing arrangement and thus a higher preserved porosity compared to that of the deformation band itself. The width of the transition zone is variable, but the combined thickness of the transition zones on each side of the band may comprise up to 50–60% of the total width of the band, similar to the 'boundary zone' described for deformation bands in porous sandstones (Antonellini and Aydin, 1994).

The SCSBs show no evidence of grain crushing or cataclasis. Instead, analysis of the high-resolution BSE images reveals textural evidence for intergranular pressure solution features at contact-points between bioclasts, seen as sutured grain contacts at various orientations within the bands (Fig. 11). The sutured contacts are evident as discrete, low-amplitude, wavy seams between adjacent grains in the deformation band. The pressure solution preferentially occurs between the echinoderm-fragments that lack internal porosity, but are occasionally observed between foraminifers and echinoderms. Additionally, there are longer, transgranular band-parallel pressure-solution seams, or stylolites, that are not restricted to individual grain contacts (Fig. 10). Intragranular fracturing of bioclasts in SCSB bands occurs (Fig. 11), but is not abundant. The scattered quartz grains in the bands remain intact and are unaffected by both pressure-solution and grain fracturing.

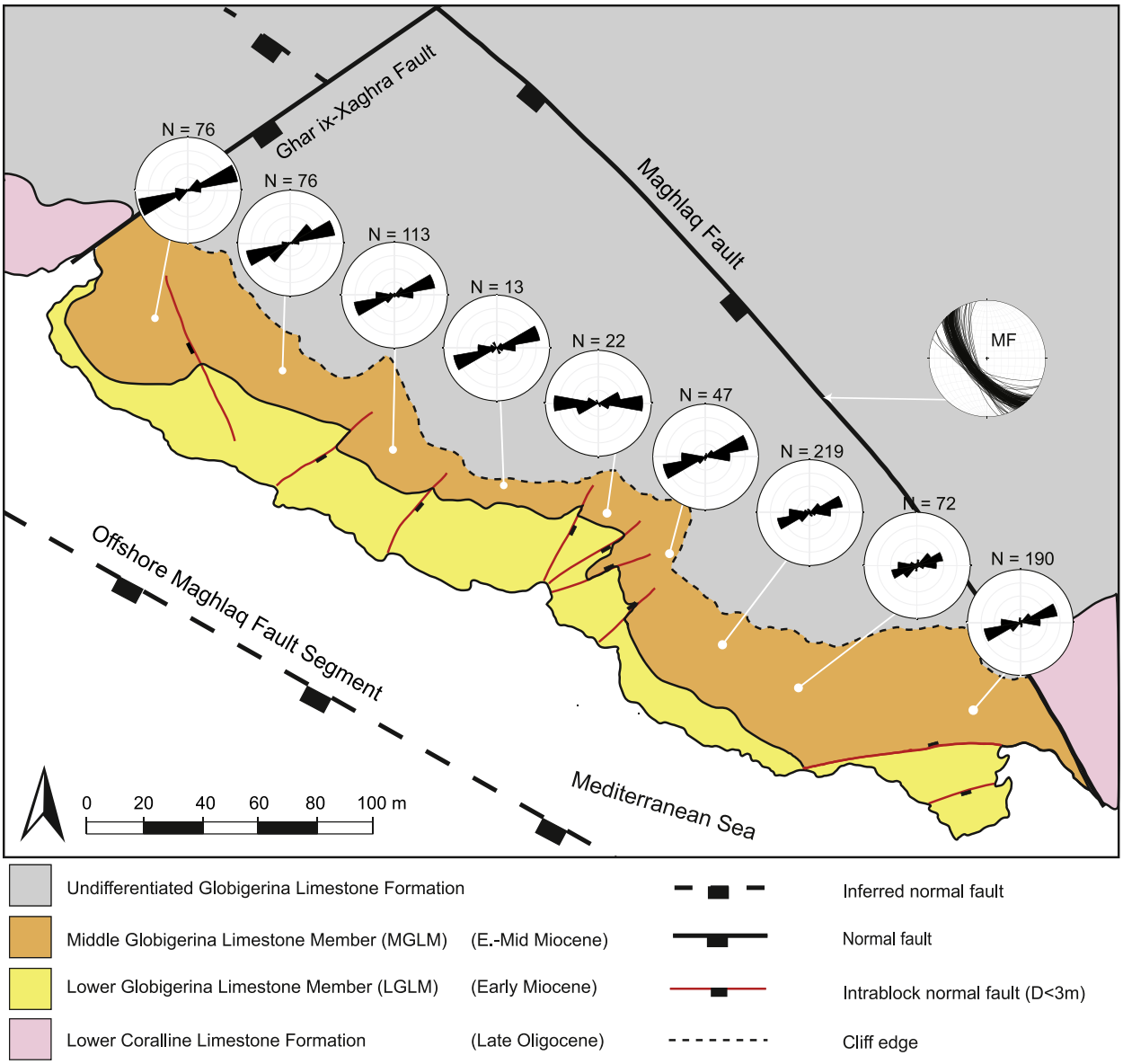

Fig. 7. Map of the study area, which is located in the hangingwall of the Maghlaq Fault. Compactive shear band (Type 2) orientation trends in the MGLM are shown using axial-symmetric rose diagrams. The equal-area and lower hemisphere projection marked 'MF' shows the NW-SE trending Maghlaq Fault. The studied outcrops are confined by the coastline and the top of the cliffs (dotted black line); the belt of outcropping MGLM wavecut platforms and cliffs terminate to the WNW and ESE at the Ghar ix-Xaghra Fault and the Maghlaq Fault, respectively. See text for details. Location is shown in Fig. 1B; the study area is also shown on satellite imagery in Fig. 2b.

6.2.2. Cataclasis-dominated compactive shear bands (type 2b)

Structures recognized as CCSB are all oriented at a high angle to the sub-horizontal sedimentary bedding. Compaction is evident as a reduction of pore space within the bands, relative to the porous host rock (Fig. 12). Similar to the SCSB, the CSCBs are separated from the surrounding host rock by a transition zone where the porosity is lower than within the host rock, but higher than inside the CSCB itself (Fig. 13). Direct evidence for shear is shown in Fig. 12, where one CCSB offsets two other CCSBs with a maximum offset of 6 mm. Transgranular fractures, oriented parallel to sub-parallel to the band-boundaries, cut across the echinoderms in the bands, whereas round foraminifers remain intact (Fig. 12C). The deformation bands exhibit significant grain-size reduction of the echinoderms in the bands, with small, highly angular echinoderm-fragments surrounding a few larger (~60 μm), survivor echinoderm-fragments (Fig. 12D and E). This is interpreted as strong evidence for cataclasis and grain crushing. Occasional grain contact suturing is observed between adjacent echinoderm-fragments (Fig. 12E), but is rare. No band-parallel transgranular pressure solution seams (Tondi et al., 2006; Cilona et al., 2012) are observed.

Grain orientation appears to be controlled by the formation of CCSBs (Fig. 13): Inside the CCSBs, the long axes of individual grains are aligned parallel to the band boundaries. In the transition zone, band-parallel grain alignment is still present but less pervasive compared to the band itself. Bioclasts in the host rock are chaotically oriented, however some grains have a parallel to sub-parallel alignment to the bedding. In sum we interpret these observations as evidence for shear-induced grain-reorientation within the CCSBs.

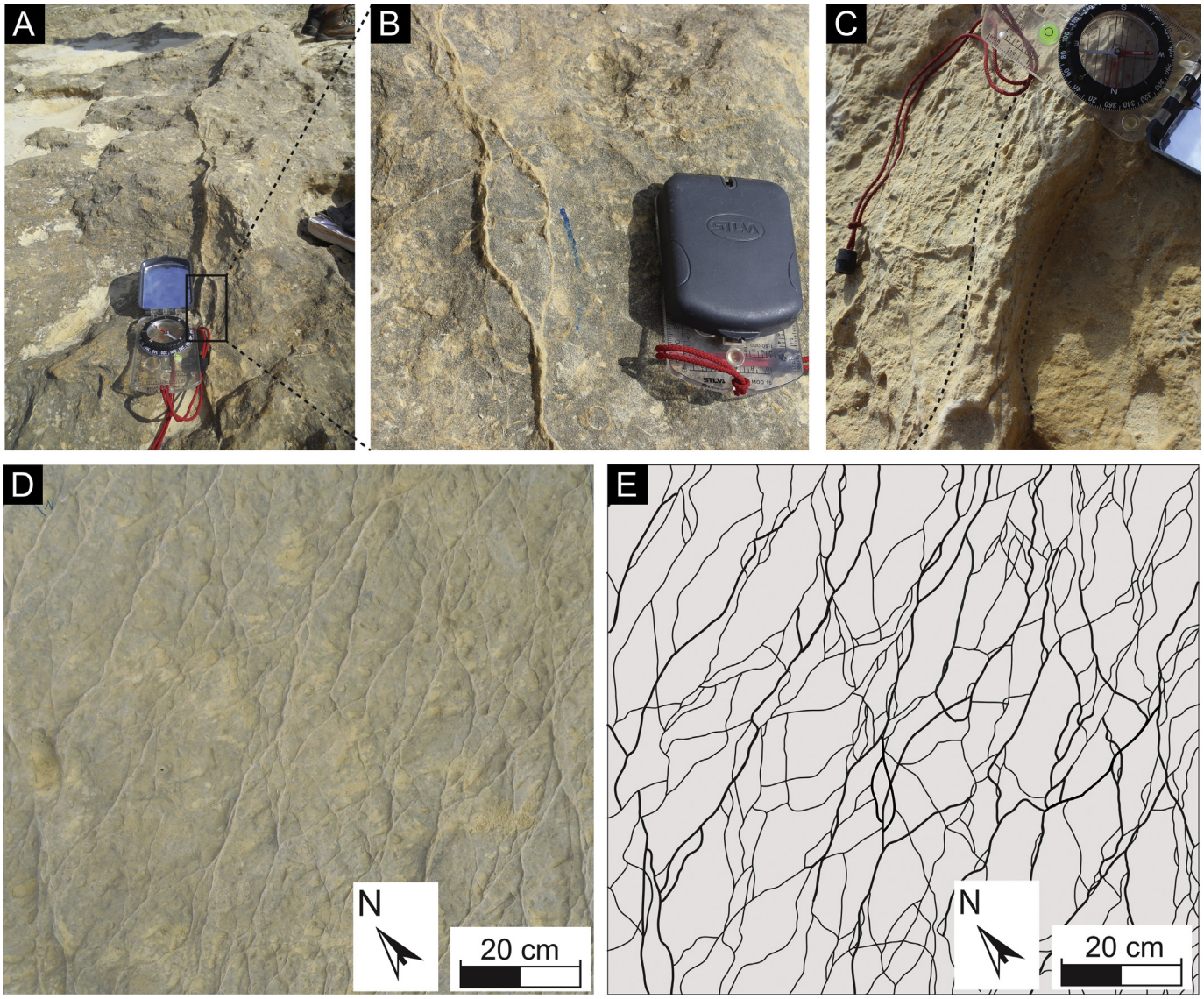

Fig. 8. Field occurrence of compactive shear bands (Type 2). (A) Single bands with occasional along-strike splays, lenses and/or relay structures. (B) Close-up of band shown in (A), locally bifurcating, enveloping a lens of intact host rock. (C) Deformation band cluster comprising approximately 10 bands. Note compass for scale. (D) Anastomosing deformation band network. (E) Line drawing of the deformation band network shown in (D). Thicker deformation bands are indicated by thicker line weight.

7. Porosity and pore size distribution

The results from the porosity measurements are shown in Fig. 14; the data are categorized as host rock, transition zone and deformation band measurements. Note that three of the 'host rock' core plug samples contained a deformation band, but given the small contribution of deformation band porosity relative to core plug total pore volume, the core plug porosity values are treated as host rock measurements.

One PCB sample was analysed (the analysed PCB is shown in Fig. 6), for which the results show that the porosity (TOP) is reduced to 1%, relative to the adjacent host rock with a porosity of 12%; however, as is evident from the images (Fig. 6B), porosity exhibits variability along strike within the band. Torabi and Fossen (2009) reported similar along-strike variability of petrophysical properties in deformation bands in sandstone.

The remaining porosity measurements are from CSB and host rock samples. The data show that the total optical porosity (TOP) shows a systematic decrease from the host rock (10–22%; mean porosity 15%), via the transition zone (7–15%; mean porosity 10%), to deformation band core (1–8%; mean porosity 3%). The porosity results from analysis of BSE imagery yielded a host rock porosity in the range of 15–31% (mean porosity 19%), and a deformation band porosity in the range of 5–12% (mean porosity 8%). Host rock porosities from core plug helium porosimetry were in the range of 17–25% (mean porosity 23%).

A porosity profile across a single CSB was made for one of the samples (Fig. 15). The profile shows a drop in porosity (TOP) from the host rock to the deformation band, via the transition zones. The porosity is reduced to 6% in the deformation band, relative to the host rock with a porosity value of 15%. Porosity in the transition zone is approximately 12%. Similar porosity across-band porosity profiles have previously been reported for deformation bands in porous sandstones (Antonellini et al., 1994; Rotevatn et al., 2008; Alikarami and Torabi, 2015).

The distinct contrast in porosity between a deformation band

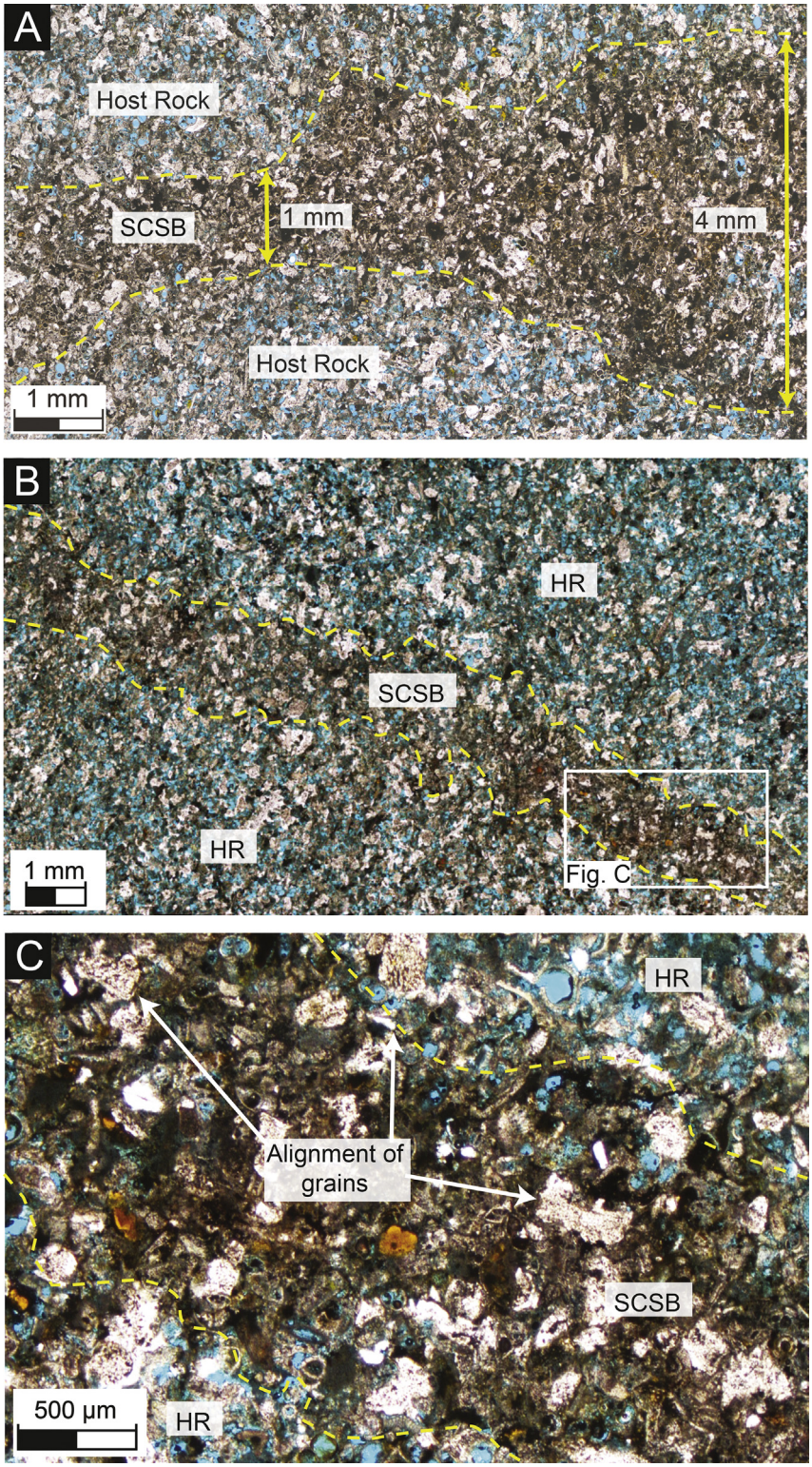

Fig. 9. Solution-dominated compactive shear band (SCSB; Type 2a) imagery. (A) Thin section photomicrograph (plane-polarized light) of SCSB, where the thickness varies notably along the length of the band (ranging from 1 to 4 mm). Porosity (blue) is markedly reduced relative to the host rock. Dotted yellow lines outline the boundary between the band and the surrounding host rock. (B) Thin section photomicrograph (plane-polarized light) of an SCSB oriented at a high angle to bedding. The average porosity (TOP) in the band is reduced to 6.7%, relative to the surrounding host rock with a porosity of 13.3%. (C) The long-axis of grains in the deformation band are aligned parallel to the boundaries of the band. SCSB = solution-dominated compactive shear band; HR = host rock. (For interpretation of the references to colour in this figure legend, the reader is referred to the web version of this article.)

and the surrounding undisturbed host rock is shown in Fig. 14B. While the host rock contains both inter- and intragranular pore space, the intergranular pore space in the deformation bands is significantly reduced. Fig. 14C presents pore-size distribution curves for a deformation band and associated host rock, separating intergranular and intragranular pore space. It is clear that the

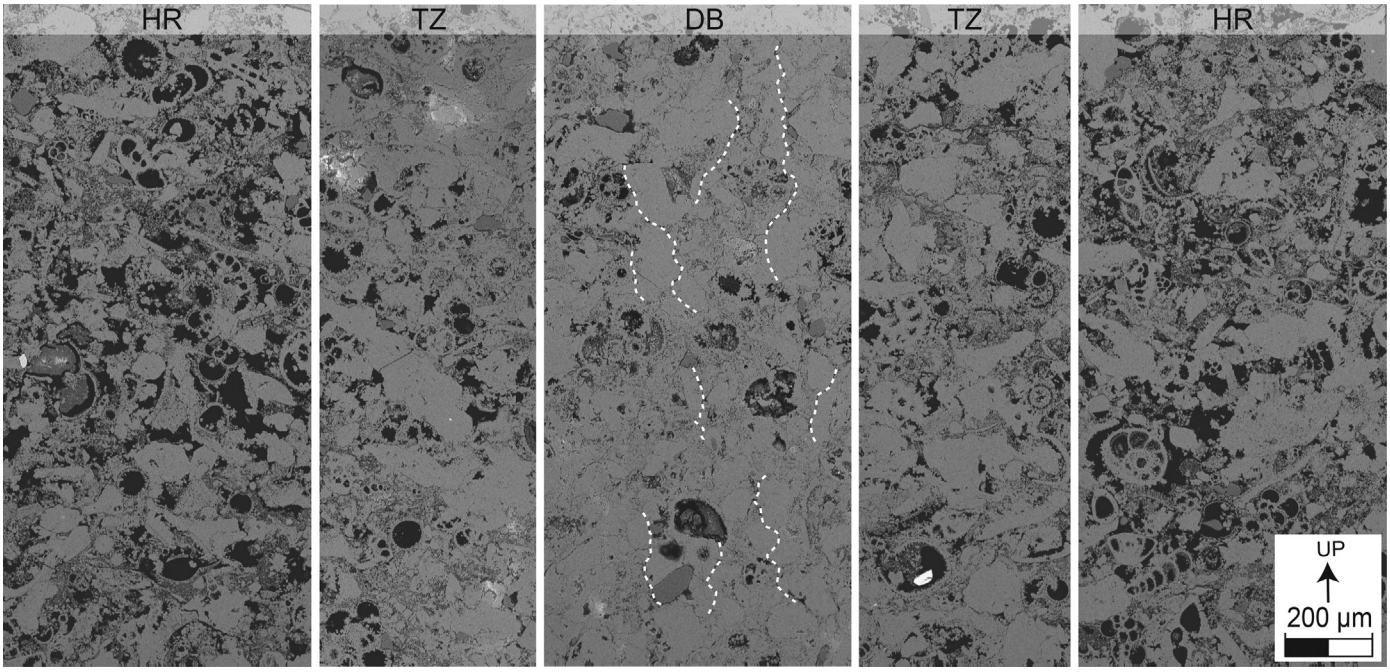

Fig. 10. Transect of BSE images, showing the progressive tighter grain packing and loss of porosity from the outermost undisturbed host rock (HR), across the transition zones (TZ) to the deformation band (DB) itself. The host rock remains unaffected by the tighter grain packing. Black areas represent pore space, while bright grey areas represent grains, matrix and cement. Note the arrow indicating stratigraphic way up. Note that sutured grain contacts and band-parallel stylolites (marked by dotted white lines) are abundant within the band, and to a lesser extent, the transition zone.

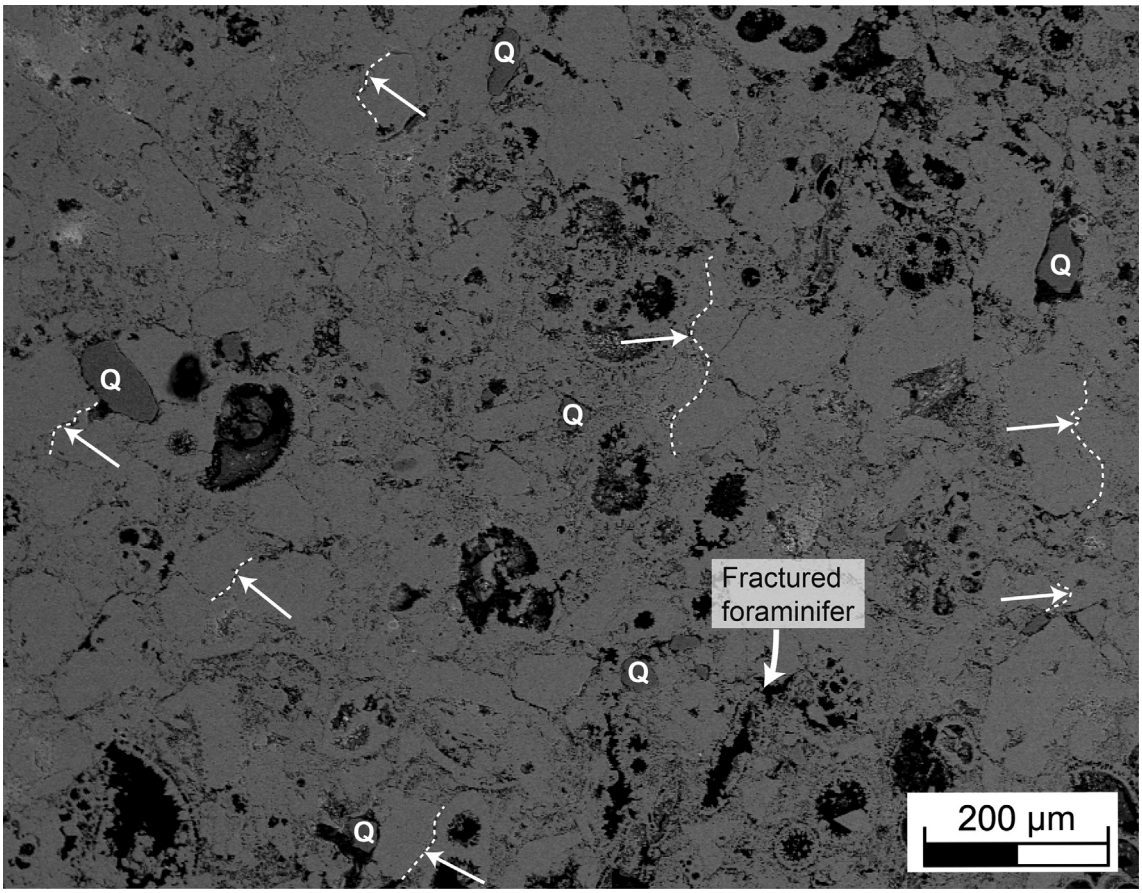

Fig. 11. BSE images of a SCSB (Type 2a), showing sutured grain contacts (indicated by arrows and dotted white lines), suggesting intergranular pressure solution affecting contacts between bioclasts in the band. Note the presence of scattered quartz grains in the deformation band and the single fractured foraminifer. Q = quartz.

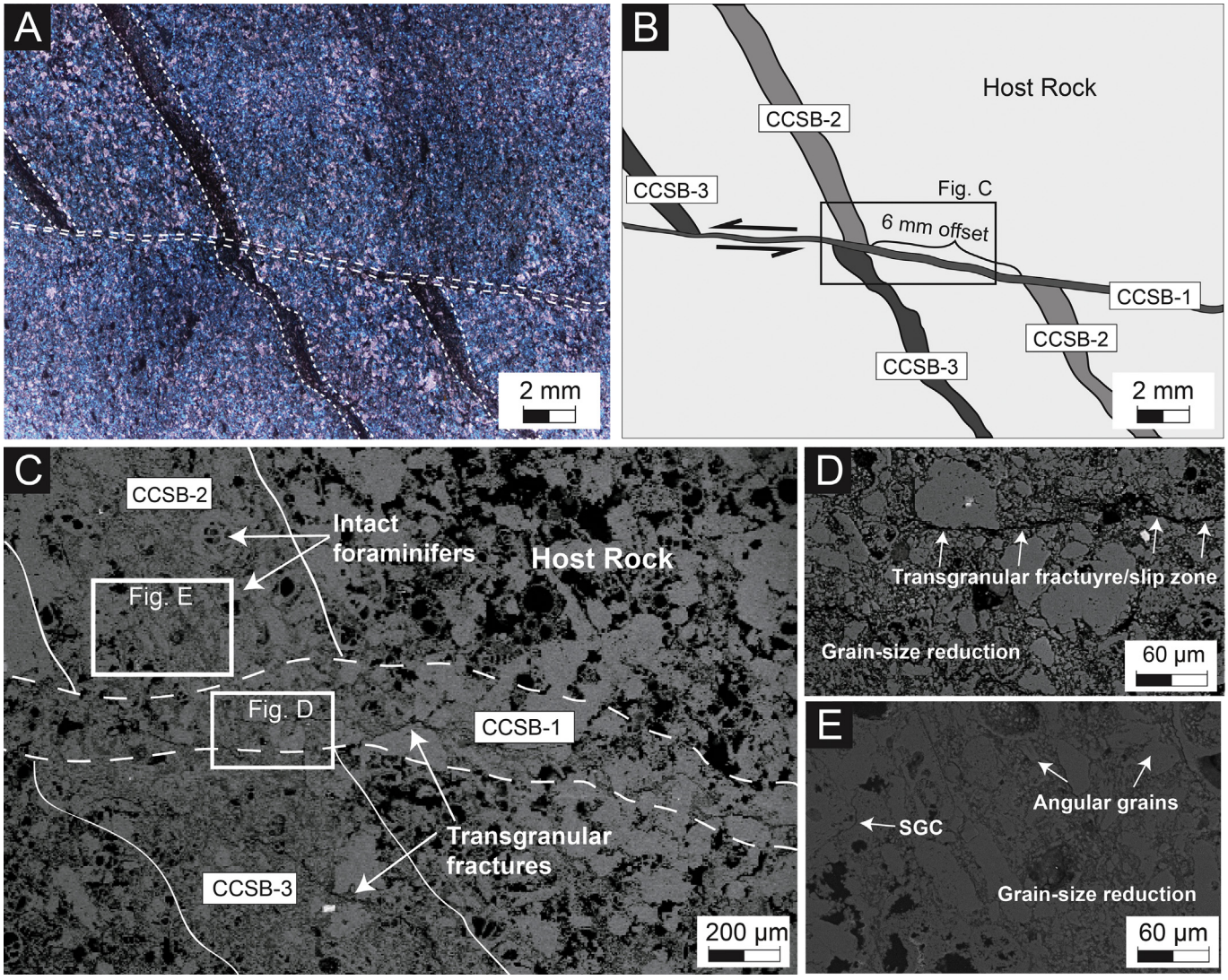

Fig. 12. Imagery of cataclastic-dominated compactive shear band (CCSB; Type 2b). (A) Thin section photomicrograph (plane-polarized light) of a CCSB offsetting two other CCSBs; a line drawing of the image is shown in (B). CCSB-1 (~200 μm thick) offsets CCSB-2 and CCSB-3 (both with a thickness ~ 600 μm), resulting in a measured displacement of 6 mm. The sense of shear is normal (stratigraphic way up is to the left). The location of (C) is indicated by a black polygon. (C) BSE image of the CCSBs shown in (A) and (B), where white arrows indicate transgranular fractures and intact foraminifers observed within the bands. The locations of D and E are indicated by the white polygons. (D) BSE image showing grain size reduction in CCSB-1. Small, angular echinoderm-fragments surround survivor grains. (E) BSE image showing highly angular grains and grain-size reduction within CCSB-2; occasional sutured grain contacts (SGC) occur but are not common.

reduction of intergranular pore space is the main contributor to the porosity reduction within the deformation band. The intragranular pore space in the deformation band is also reduced, but to a lesser extent than the intergranular pore space.

8. Discussion

8.1. Growth and temporal evolution of the studied deformation bands

Based on the geometric relations between different structures we here interpret their temporal evolution (Fig. 16). PCBs were the first deformation bands to form, based on the abutment of CSBs against the PCBs. Based on observations presented earlier, we suggest that one of the three following models may account for how the sub-horizontal, bedding-parallel PCBs formed: (1) PCBs formed widely due to general burial-induced vertical loading (cf. Aydin and Ahmadov, 2009); in this model, the PCBs did not form tectonically and are not spatially restricted to, or related to, the growth of the Maghlaq Fault; (2) PCBs formed due to tectonic stresses during growth of the Maghlaq Fault; here, a vertical maximum stress direction during extensional faulting is responsible for PCB formation; (3) a hybrid model is that the PCBs formed by burial-induced vertical loading (i.e. same principal driving mechanism), but that PCB formation was local to the subsiding hangingwall of the MF (and likely also other active syn-rift faults), where subsidence rates were higher than elsewhere; due to the role of faulting in controlling hangingwall subsidence (and hence the location of PCB formation), we refer to this third model as a 'semi-tectonically controlled' model. Two key observations argue against the first hypothesis: (i) PCBs appear only to be present within the MGLM *in the hangingwall* of the MF, and (ii) the MGLM is a syn-rift unit whose thickness is variable and whose burial was controlled by faults (Dart et al., 1993). These points strongly suggest that PCB formation was, spatially and temporally, related to the MF.

Now that we have established that the PCBs are somehow

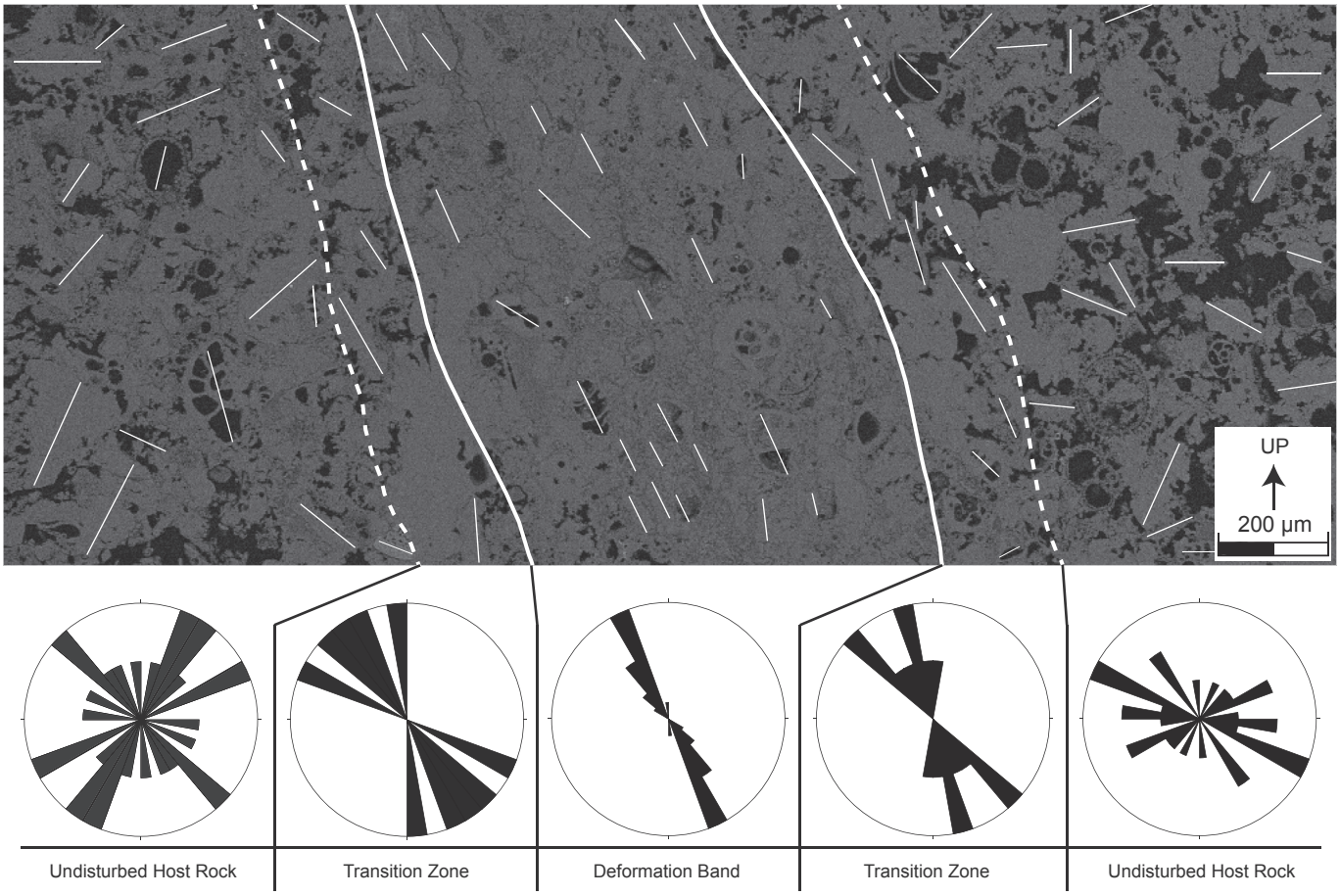

Fig. 13. BSE image and symmetric rose diagrams documenting the alignment of bioclasts (marked by short, white lines) in the undisturbed host rock, transition zone and the deformation band. The long-axis of bioclasts in the deformation band are aligned parallel to boundaries of the band. The dashed white line delineates the boundary between host rock and the transition zone, whereas white solid line represents the boundary between the transition zone and deformation band. Note the black arrow indicating stratigraphic way up.

related to the MF, a key question arising is "was compaction localization driven by burial-induced vertical loading during progressive hangingwall subsidence of the MF, or by the tectonic stresses that drove extensional faulting?". Based on the early formation of the PCBs, and the fact that bed-parallel PCBs are generally considered to form in response to the overburden (Tondi et al., 2006; Agosta et al., 2009; Aydin and Ahmadov, 2009), we favour burial-induced vertical loading, albeit local to the fault-controlled MF hangingwall depocentre (hypothesis 3 above, i.e. the 'hybrid model'), as the most plausible model for the formation of PCBs in the study area. Although PCB *formation* is controlled by burial-induced loading, a (semi-)tectonic control on PCB *localization/distribution* is thus documented for the first time in an extensional setting; PCBs have previously only been related to (i) wholesale burial-induced localization of compaction (op. cit.), or (ii) contraction (e.g. Mollema and Antonellini, 1996; Fossen et al., 2011).

CSBs formed after PCBs (Fig. 16), based on the above mentioned abutment relations. The high CSB frequencies near the MF and intrablock faults suggest that they are all somehow related, however the fact that deformation bands are chiefly orientated oblique to the MF and sub-parallel to the intrablock faults raises the question; "what is the spatiotemporal relationship between the MF, the intrablock faults and the CSBs?". In our attempt to address this question, we considered the following three hypotheses: (i) CSBs formed unrelated to fault formation in the study area; (ii) the MF and the intrablock faults formed at different times during different tectonic events, and CSBs formed during one of these events; (iii) the MF, the intrablock faults and the CSBs formed more-or-less coevally during one single stress regime. The first two hypotheses are ruled out by the observations that (i) *both* the MF *and* the intrablock faults are associated with high CSB frequency in their damage zones; (ii) the CSBs are orientated sub-parallel to the intrablock faults; (iii) deformation bands in the Globigerina Limestone Formation appears to be exclusively localized to the hangingwall of the MF; and (iv) there is no evidence to support multiple tectonic events affecting the studied extensional fault array; on the contrary evidence indicates that the MF, and indeed Malta as a whole, is characterized by the Pantelleria rifting event alone, with no evidence of later reactivation (Dart et al., 1993; Bonson et al., 2007; Putz-Perrier and Sanderson, 2010). We therefore conclude that the third hypothesis is more likely, namely that MF, the intrablock faults and the CSBs formed more-or-less coevally.

Having established this, there is still an outstanding question of why the CSBs (and the intrablock faults) display such an oblique strike relative to the MF (Fig. 7). We suggest that this may be explained by the localization of the studied outcrop between two overlapping segments of the left-stepping MF, where one segment is located onshore in the study area, and one is located immediately outboard of the study area as indicated by Bonson et al. (2007) and shown in Figs. 2 and 7. The orientation of the intrablock faults and the CSBs agree well with the typical orientation of structures growing in a locally perturbed stress field between two overlapping, left-stepping fault segments (cf. Crider and Pollard, 1998;

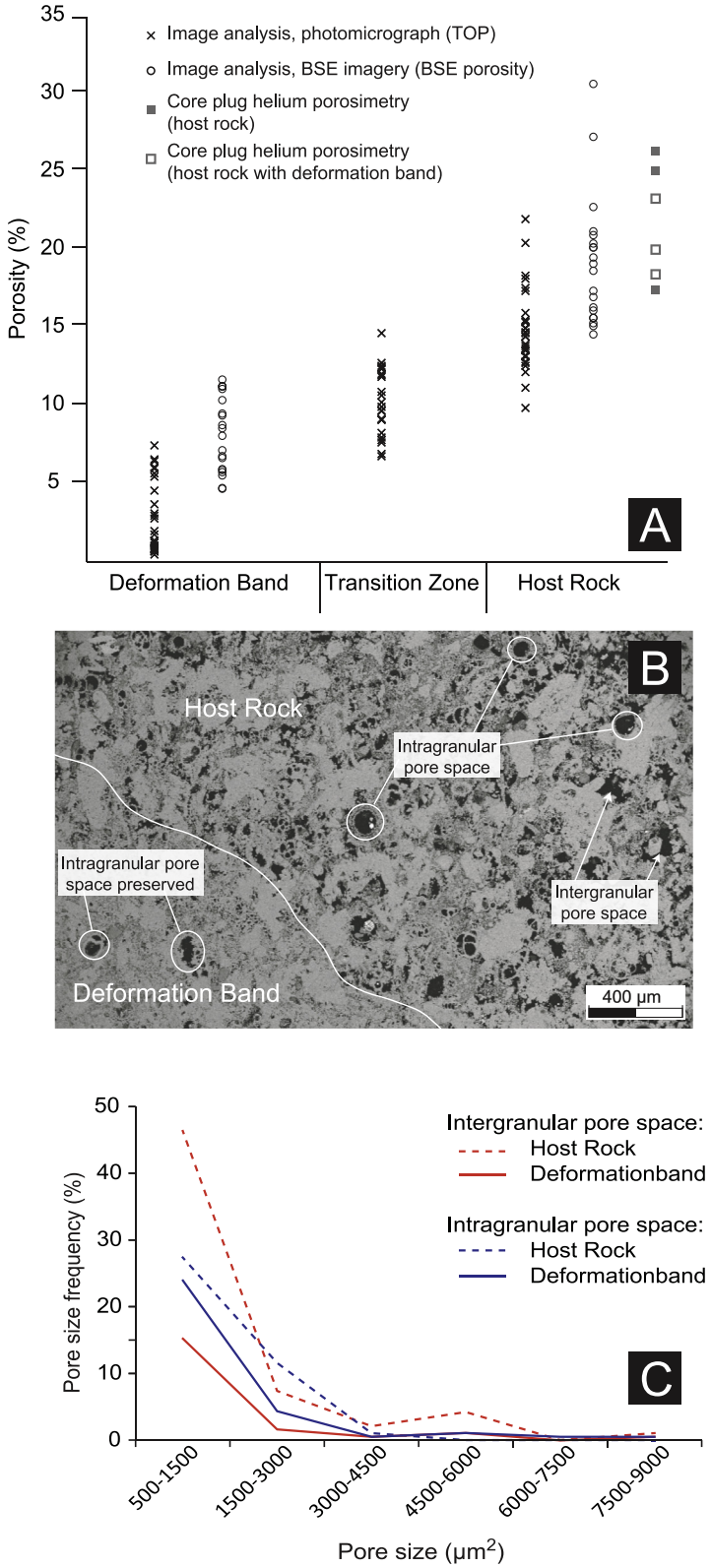

Fig. 14. (A) Total optical porosities (TOP), BSE porosities, and core plug porosities determined for sampled deformation bands, transition zones and host rocks. Note that three of the 'host rock' core plug samples contained a deformation band, but given the small contribution of deformation band porosity relative to core plug total pore volume, the core plug porosity values are treated as host rock measurements. (B) Binary BSE image showing that the *intergranular* pore space in the deformation band is significantly reduced relative to the host rock. The *intragranular* pore space in the deformation band is better preserved. This is confirmed by (C) pore-size distribution curves for a CSB and associated host rock: the intergranular pore space is significantly reduced within the deformation bands, whereas the intragranular pore space is better preserved. The plotted values refer to pores with a larger pore size area than 500 μm^2, which is in this paper is defined as the boundary between macro- and micropores and corresponds with a pore length of c. 30 μm.

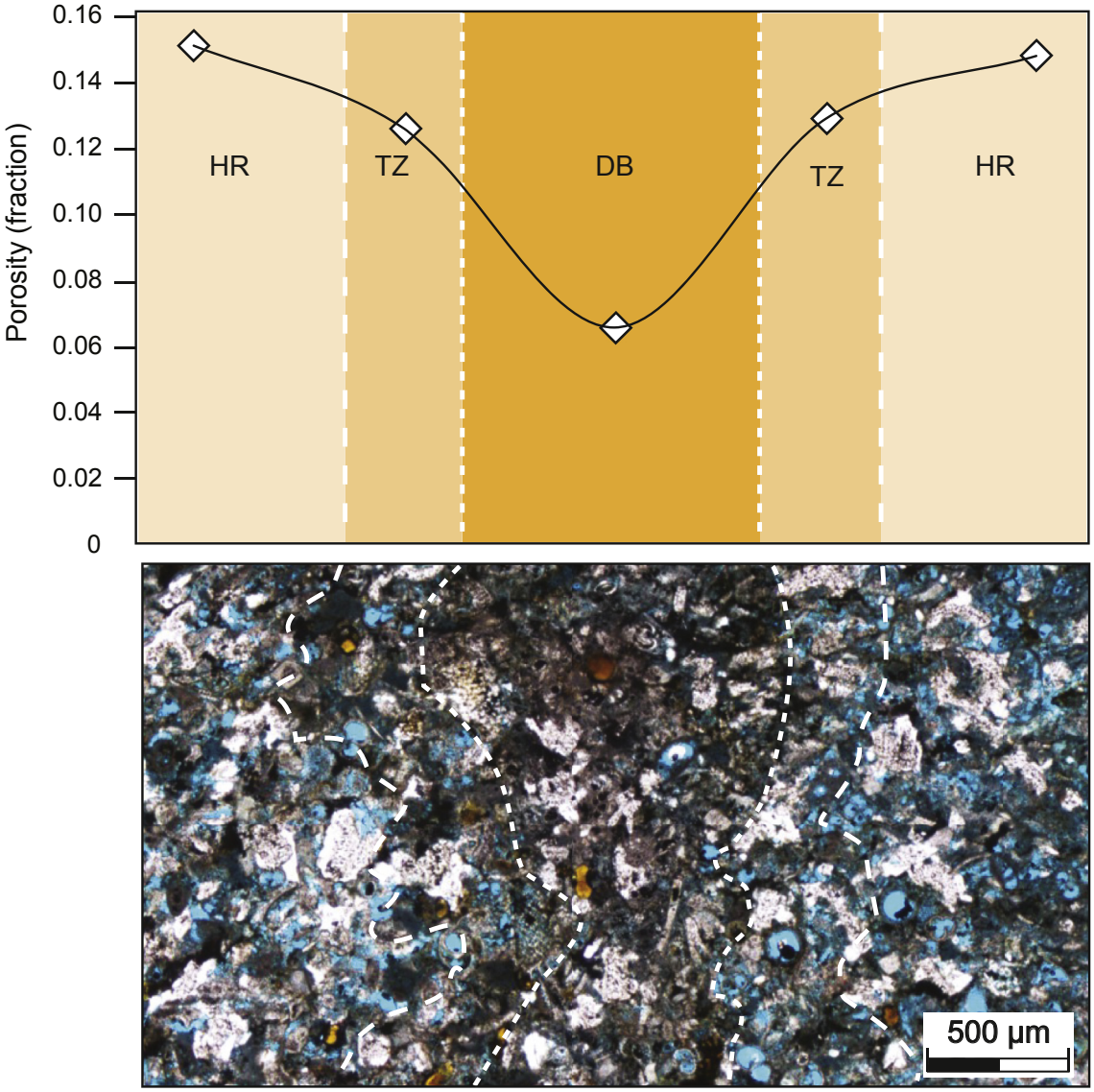

Fig. 15. Thin section photomicrograph (plane-polarized light) and porosity profile across a single SCSB, showing the decrease in porosity from the host rock (HR), via the transition zones (TZ) to the deformation band (DB).

Kattenhorn et al., 2000; Bastesen and Rotevatn, 2012; Rotevatn and Bastesen, 2014). An argument against this would be that one would expect to see more scatter in orientations if the structures grew in a perturbed stress field (cf. Fossen et al. 2005; Rotevatn et al., 2007); however, this is not always be the case and there are examples where structures growing between overlapping faults follow a more systematic pattern like the one seen in the current study (e.g. Peacock and Parfitt, 2002; Faure Walker et al., 2009).

An alternative hypothesis is that the intrablock faults and the CSBs grew as Riedel shears (sensu Sylvester, 1988) between the overlapping MF fault segments. However, Riedel shears in a normal fault system would strike more or less parallel to the main fault trend, so to invoke Riedel shearing one would need to prove significant strike-slip movement on the system. Both the Maghlaq Fault and the subsidiary IBFs (which are parallel to the CSB orientations) show a predominantly normal-sense shear (also supported by Bonson et al., 2007). In summary therefore, we find it hard to reconcile these structures with the Riedel shear hypothesis.

Our preferred interpretation is therefore that CSBs and the intrablock faults formed under locally perturbed stresses within the overall tensional stress regime as segments of the extensional MF array grew, overlapped and, locally, linked (cf. Fossen and Rotevatn, 2016).

On the temporal relationship between the two different types of CSBs, cross-cutting relations in the field do not allow us to conclude a relative sequence of formation between CCSBs and SCSBs. Given the lack of conclusive evidence from cross-cutting relations, we find it likely that SCSBs and CCSBs formed more-or-less coevally.

8.2. Deformation mechanisms

Microstructural evidence suggest that within PCBs, grain reorganization and pressure solution were responsible for accommodating strain localization, similar to what has been suggested by previous authors (Rustichelli et al., 2012).

Within CSBs, we have identified bands that are dominated by pressure-solution (SCSB), and bands that are dominated by cataclasis (CCSB). The two types of CSBs occur together across the study

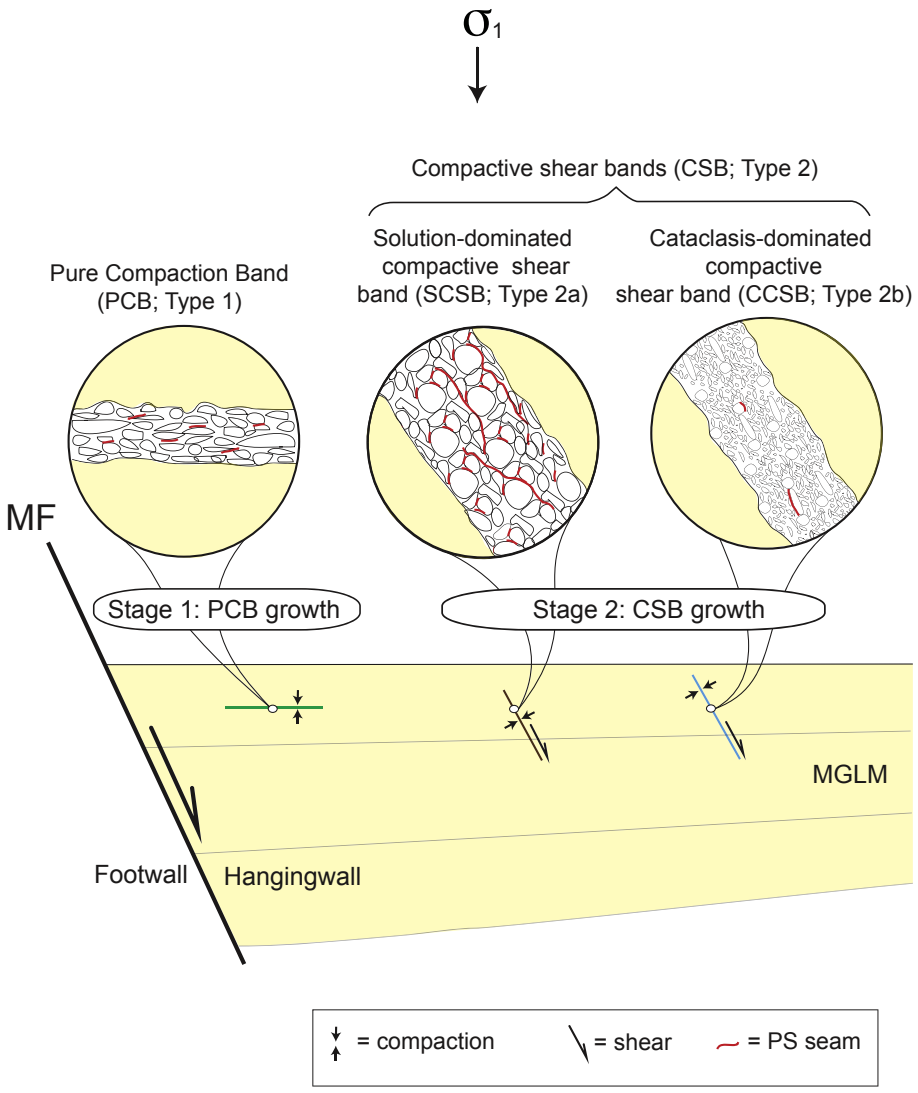

Fig. 16. Conceptual model for the evolution of the studied deformation bands. Stage 1: The Maghlaq Fault is active, and vertical loading related to the syn-kinematic accumulation of the MGLM leads to PCB formation restricted to the hangingwall depocentre of the Maghlaq Fault. Grain reorganization aided by minor grain boundary dissolution (pressure solution) are the chief mechanisms for strain accommodation. Stage 2: During continued growth of the Maghlaq Fault, CSBs form in its hangingwall, accommodating compaction and shear. Chief mechanisms for strain accommodation are grain boundary dissolution (pressure solution) in SCSBs, and cataclasis within CCSBs. MGLM = Middle Globigerina Limestone Formation; PCB = pure compaction band; CSB = compactive shear band; SCSB = solution-dominated compactive shear band; CCSB = cataclasis-dominated compactive shear band; PS = pressure solution.

area and are not spatially separated into different areas in which either of the two occur exclusively. The preferential alignment of elongated grains parallel to the borders of the SCSBs (Fig. 9C) indicates that shear and compaction in the bands initially were accommodated by granular flow mechanisms, involving grain translation and rotation of bioclasts, and, subsequently, pore collapse by pressure solution. Within CCSBs, on the other hand, cataclasis (i.e. grain crushing) is the chief deformation mechanism (as evidenced by an abundance of small, highly angular clasts surrounding survivor grains, see Fig. 12), with only a smaller component of pressure solution processes being evident. Tondi et al. (2006) argue that, contrary to sandstones where grain fracturing and crushing is the chief mechanism in cataclasis (Engelder, 1974; Aydin, 1978; Wong, 1990), grain size reduction in CSBs in carbonates is achieved by pressure solution and subsequent shearing of stylolites. This contrasts the findings of this study, where we did not find supporting evidence for extensive stylolite shearing being responsible for brittle grain size reduction through grain crushing. Instead, the bands displaying cataclasis exhibit widespread evidence for distributed grain comminution in the form of highly angular grains in a range of sizes smaller than the overall host rock grain size (Fig. 12). Rath et al. (2011) also reported cataclastic deformation bands in carbonate grainstones without evidence for extensive pressure solution processes, suggesting cementation (yet preservation of high porosities) led to the transitioning from grain reorganization to cataclasis by increasing the yield strength of the host rock. We do not see evidence for a relationship between cementation and onset of cataclasis in the present study, since SCSBs and CCSBs appear to have formed coevally, and since there is no discernible contrast in the amount or spatial distribution of cement in the study area. Nevertheless, our finds, and those of Rath et al. (2011), raise the question of the relative importance of pressure solution vs. brittle grain crushing as mechanisms for reducing grain size in deformation bands in porous carbonate rocks. Cilona et al. (2012) argue that, generally in nature, shearing of carbonate deformation bands may take place without significant grain crushing, and that grain contacts exhibit a more ductile behaviour than that seen in experiments. This would be a reasonable

description of the SCSBs of the present study too. The observations of the CCSBs, however, indicate that cataclasis in some cases may occur independent of pressure solution processes/features, and that grain size reduction may take place through grain fracturing and splitting caused by stress concentration at grain contact points, similar to the processes seen in deformation bands in sandstone (e.g. Antonellini et al., 1994).

The studies that report stylolite shearing as an important process for promoting cataclasis also describe extensive occurrence of stylolites evident at the outcrop scale in the host rocks (e.g. Tondi et al., 2006; Cilona et al., 2012; Rustichelli et al., 2012). This is not the case in the present study, which may suggest that pressure solution processes are of less importance in the present study area compared to areas studied by previous authors. One possible explanation is that the present study area is in an extensional tectonic setting, whereas most previous studied areas are characterized by contraction (Table 1 and references therein). In general, stylolites may be more abundant in contractional tectonic settings since they may form due to both burial (bed-parallel solution stylolites) and in response to the sub-horizontal greatest principal stress (bed-normal stylolites). This therefore begs the question "Could pressure-solution processes be of less importance for facilitating grain size reduction in extensional tectonic settings compared to contractional tectonic settings, where pressure solution processes evidently play a large role?" A parallel that may lend support to this view can be found in studies of the relationship between faulting and pressure-solution seams. These studies suggest that pre-existing (earlier, belonging to a previous event) or precursor (incipient features during same event) pressure-solution seams may facilitate the localization, nucleation, propagation and linkage mainly of thrusts, transpressional faults (Crider and Peacock, 2004) or fractures/faults forming at contractional step-overs (Ohlmacher and Aydin, 1997; Willemse et al., 1997; Crider and Peacock, 2004), whereas normal faults are generally associated with the opposite, i.e. pressure solution seams exploiting pre-existing faults and fractures (Peacock et al., 1998). What can be drawn from this is that stylolites seem to be relatively more important for the nucleation and growth of thrust and strike-slip faults, while stylolites tend to be secondary in normal faulting. We suggest that a similar relationship may exist for deformation bands, i.e. that grain size reduction in contractional settings may be more dependent on pressure solution processes (sensu Tondi et al., 2006; Cilona et al., 2012) compared to extensional settings. Obviously, more work on deformation bands in carbonate rocks in extensional tectonics settings would be needed in order to rigorously test this idea.

8.3. *Effects of host rock variability on deformation mechanisms and strain localization*

Host rock variability impacts the localization, style and mechanisms of deformation on a range of scales:

(1) On a semi-regional scale, the Globigerina Limestone Formation laterally grades to finer-grained micrite-dominated limestones near the Victoria Lines Fault (Fig. 1), c. 20 km WNW of our study area, where deformation appears to be accommodated by joints and faults rather than deformation bands (Michie et al., 2014; Michie, 2015; and supported by our own observations in that area).
(2) On a more local scale, the localization of PCBs in a retracted and slightly finer-grained portion of the studied succession (see Figs. 6b and 9c for a comparison of the grain sizes in the host rocks of PCBs and CSBs, respectively) suggests that finer grain sizes, or grain size distribution (see Cheung et al., 2012), may promote compaction localization. This interpretation is supported by the findings of Rustichelli et al. (2012), who reported that finer-grained, better-sorted grainstones with spherical grains promoted compaction banding, contrary to what was suggested by Tondi et al. (2006). Cheung et al. (2012) argue that grain size distribution, rather than grain size, is a controlling factor for PCB localization. Regardless of whether it pertains to finer grain sizes or the actual grain size distribution, the broader reason why PCBs are limited to a 30-cm interval and thus not widely distributed within the study area seems to be clearly relatable to changes in host rock properties. PCBs are extremely sensitive to changes in porosity, grain size (Rustichelli et al., 2012), grain size distribution (Cheung et al., 2012), shape and sorting (e.g. Schultz et al., 2010), and thus preferentially localized where conditions for compaction banding were ideal (cf. Cilona et al., 2014).
(3) As observed in the CCSBs of this study (Fig. 12), the angular echinoderm-fragments are affected by cataclasis, whereas the foraminifers appear more resilient and remain intact. (Vajdova et al., 2012 similarly reported that allochems survived experimental inelastic compaction, whereas the matrix underwent microcracking). This may be linked to the fact that, due to their solid shell framework and spherical shape, the foraminifers are less prone to crushing; this also means that intragranular porosity within foraminifer chambers are generally well preserved. However, due to high angularity and size, the echinoderms are more easily affected by cataclasis. The angularity of the echinoderms allows for higher stress concentration to arise across sharp contact points, and promotes grain interlocking and resistance to grain rolling. At the same time, echinoid fragments promote the growth of syntaxial cements, which may strengthen grain contacts (Cilona et al., 2014) and further promote stress concentration and cataclasis. The reduction in grain-size of the echinoderms (and subsequent closer packing of grains) in turn allows for larger surface areas for pressure solution to occur (cf. Croizé et al., 2010; Cilona et al., 2012). Hence, we speculate that the cataclasis may have catalysed the growth of the (admittedly very few) grain-scale solution seams observed within the studied CCSBs.
(4) A final observation is that deformation bands do not develop in the bioturbated parts of the studied succession, but are generally abundant in the non-bioturbated parts. It is well known that bioturbation can physically alter sediments by mixing, homogenization, compaction, dewatering and more (Taylor and Goldring, 1993). Such changes may occur at a minute scale where sand grains are shifted, or on a macro-scale where entire bedforms are reworked. Given the sensitivity of deformation bands to even small changes in prosity, grain size and sorting (e.g. Fossen et al., 2007), we suggest such alterations of the host rock may demote deformation band formation, thus explaining the absence of deformation bands in the intervals affected by intense bioturbation.

9. Conclusions

We have documented, for the first time, deformation bands developing in the hangingwall syn-rift depocentre of an active growth fault. Two main types of deformation bands were identified; pure compaction bands (PCBs) and compactive shear bands (CSBs), of which the latter is comprised of two distinct sub-types dominated by pressure-solution (solution-dominated compactive

shear bands; SCSB) and cataclasis (cataclasis-dominated compactive shear bands; CCSB), respectively. The main conclusions of this study are listed below:

- PCBs and CSBs formed sequentially during syn-rift sedimentation and growth of the MF during the Pantelleria rifting event (one single tectonic event); PCBs formed first due to early fault-controlled burial in the hangingwall of the MF; CSBs formed subsequently in a perturbed stress field during growth and interaction of MF segments.
- Burial-induced vertical loading local to tectonically-controlled syn-rift depocentres is responsible for the PCB formation. A (semi-)tectonic control on the distribution of PCB is thus documented, for the first time in an extensional setting.
- Grain reorganization and pressure solution processes are the dominant deformation mechanisms within PCBs.
- Pressure-solution and cataclasis are the chief deformation mechanisms responsible for CSB formation. Contrary to findings of many previous authors (e.g. Tondi, 2007; Rustichelli et al., 2012), the two processes here appear to have operated separately rather than in concert, with pressure solution dominating SCSBs, and cataclasis dominating CCSBs.
- Cataclasis (i.e. grain fracturing and grain crushing) is not associated with stylolite shearing (cf. Tondi et al., 2006); instead, cataclasis is widespread within the CCSBs and associated with grain fracturing and mechanical grain comminution.
- Cataclasis in CCSBs preferentially affects echinoid fragments, since their highly angular shape promotes grain interlocking and demotes non-destructive granular flow
- We suggest that, whereas pressure solution is a significant process for grain size reduction within deformation bands in carbonate grainstones in contractional tectonic regimes, pressure solution processes may be relatively less important in extensional regimes. We caveat, however, that more research into deformation bands in carbonate rocks in extensional tectonic settings is needed to rigorously test this proposition.
- Bioturbated grainstones are not prone to deformation banding. Given the inherent reorganization and disturbance of sediments caused by bioturbation, and given that deformation bands are highly sensitive to host rock property changes, the intervals affected by pervasive bioturbation are rendered unsuitable for deformation band formation.

Acknowledgements

Marco Antonellini and an anonymous reviewer are thanked for their constructive and insightful reviews, which led to significant improvements to this paper. Editor Toru Takeshita is thanked for excellent editorial guidance. Chris Bonson thanked for generously sharing his knowledge, and for directing us to a range of interesting outcrops in the Maltese Islands. We are grateful to Chris Dart, who provided helpful input and discussions on Maltese geology at an early stage of this project. Cathy Hollis and Catherine Breislin at the University of Manchester are thanked for helping with the porosity measurements. We are also grateful to Håvard Flatebø Trætteberg for assistance and entertainment in the field. Professor Carmelo Agius of the University of Malta, and his wife Anna Agius, are thanked for providing us with a home away in Malta. We acknowledge funding from BKK and the University of Bergen through two student grants to E. Thorsheim and H.S.S. Fossmark, awarded through the BKK-UiB agreement for utilization of renewable energy, energy restructuring and future-oriented infrastructure.

References

Agosta, F., Alessandroni, M., Tondi, E., Aydin, A., 2009. Oblique normal faulting along the northern edge of the Majella Anticline, central Italy: inferences on hydrocarbon migration and accumulation. J. Struct. Geol. 31, 674–690.
Alikarami, R., Torabi, A., 2015. Micro-texture and petrophysical properties of dilation and compaction shear bands in sand. Geomech. Energy Environ. 3, 1–10.
Antonellini, M., Aydin, A., 1994. Effect of faulting on fluid flow in porous sandstones: petrophysical properties. AAPG Bull. 78, 355–377.
Antonellini, M., Aydin, A., Pollard, D.D., 1994. Microstructure of deformation bands in porous sandstones at Arches National Park, Utah. J. Struct. Geol. 16, 941–959.
Antonellini, M., Cilona, A., Tondi, E., Zambrano, M., Agosta, F., 2014a. Fluid flow numerical experiments of faulted porous carbonates, Northwest Sicily (Italy). Mar. Pet. Geol. 55, 186–201.
Antonellini, M., Petracchini, L., Billi, A., Scrocca, D., 2014b. First reported occurrence of deformation bands in a platform limestone, the Jurassic Calcare Massiccio Fm., northern Apennines, Italy. Tectonophysics 628, 85–104.
Antonellini, M., Tondi, E., Agosta, F., Aydin, A., Cello, G., 2008. Failure modes in deep-water carbonates and their impact for fault development: Majella Mountain, Central Apennines, Italy. Mar. Pet. Geol. 25, 1074–1096.
Antonellini, M.A., Pollard, D.D., 1995. Distinct element modeling of deformation bands in sandstone. J. Struct. Geol. 17, 1165–1182.
Argnani, A., 1990. Geophysics of the Mediterranean BasinThe strait of sicily rift zone: foreland deformation related to the evolution of a back-arc basin. J. Geodyn. 12, 311–331.
Aydin, A., 1978. Small faults formed as deformation bands in sandstone. Pageoph 116, 913–930.
Aydin, A., Ahmadov, R., 2009. Bed-parallel compaction bands in aeolian sandstone: their identification, characterization and implications. Tectonophysics 479, 277–284.
Aydin, A., Borja, R.I., Eichhubl, P., 2006. Geological and mathematical framework for failure modes in granular rock. J. Struct. Geol. 28, 83–98.
Aydin, A., Johnson, A.M., 1978. Development of faults as zones of deformation bands and as slip surfaces in sandstone. Pageoph 116, 931–942.
Aydin, A., Johnson, A.M., 1983. Analysis of faulting in porous sandstones. J. Struct. Geol. 5, 19–31.
Ballas, G., Soliva, R., Sizun, J.-P., Benedicto, A., Cavailhes, T., Raynaud, S., 2012. The importance of the degree of cataclasis in shear bands for fluid flow in porous sandstone, Provence, France. AAPG Bull. 96, 2167–2186.
Balsamo, F., Storti, F., 2011. Size-dependent comminution, tectonic mixing, and sealing behavior of a "structurally oversimplified" fault zone in poorly lithified sands: evidence for a coseismic rupture? Geol. Soc. Am. Bull. 123, 601–619.
Bastesen, E., Rotevatn, A., 2012. Evolution and structural style of relay zones in layered limestone–shale sequences: insights from the Hammam Faraun Fault Block, Suez rift, Egypt. J. Geol. Soc. 169, 477–488.
Baud, P., Meredith, P., Townend, E., 2012. Permeability evolution during triaxial compaction of an anisotropic porous sandstone. J. Geophys. Res. Solid Earth 117 (n/a-n/a).
Baud, P., Schubnel, A., Wong, T.-f., 2000. Dilatancy, compaction, and failure mode in Solnhofen limestone. J. Geophys. Res. Solid Earth 105, 19289–19303.
Baud, P., Vinciguerra, S., David, C., Cavallo, A., Walker, E., Reuschlé, T., 2009. Compaction and failure in high porosity carbonates: mechanical data and microstructural observations. In: Vinciguerra, S., Bernabé, Y. (Eds.), Rock Physics and Natural Hazards. Birkhäuser Basel, pp. 869–898.
Baxevanis, T., Papamichos, E., Flornes, O., Larsen, I., 2006. Compaction bands and induced permeability reduction in Tuffeau de Maastricht calcarenite. Acta Geotech. 1, 123–135.
Bense, V.F., Van den Berg, E.H., Van Balen, R.T., 2003. Deformation mechanisms and hydraulic properties of fault zones in unconsolidated sediments; the Roer Valley Rift System, The Netherlands. Hydrogeol. J. 11, 319–332.
Bonson, C.G., Childs, C., Walsh, J.J., Schöpfer, M.P.J., Carboni, V., 2007. Geometric and kinematic controls on the internal structure of a large normal fault in massive limestones: the Maghlaq Fault, Malta. J. Struct. Geol. 29, 336–354.
Cashman, S., Cashman, K., 2000. Cataclasis and deformation-band formation in unconsolidated marine terrace sand, Humboldt County, California. Geology 28, 111–114.
Cello, G., Crisci, G.M., Marabini, S., Tortorici, L., 1985. Transtensive tectonics in the Strait of Sicily: structural and volcanological evidence from the island of Pantelleria. Tectonics 4, 311–322.
Chemenda, A.I., Wibberley, C., Saillet, E., 2012. Evolution of compactive shear deformation bands: numerical models and geological data. Tectonophysics 526–529, 56–66.
Cheung, C.S.N., Baud, P., Wong, T.-f., 2012. Effect of grain size distribution on the development of compaction localization in porous sandstone. Geophys. Res. Lett. 39 (n/a-n/a).
Choquette, P.W., Pray, L.C., 1970. Geologic nomenclature and classification of porosity in sedimentary carbonates. AAPG Bull. 54, 207–244.
Cilona, A., Baud, P., Tondi, E., Agosta, F., Vinciguerra, S., Rustichelli, A., Spiers, C.J., 2012. Deformation bands in porous carbonate grainstones: field and laboratory observations. J. Struct. Geol. 45, 137–157.
Cilona, A., Faulkner, D.R., Tondi, E., Agosta, F., Mancini, L., Rustichelli, A., Baud, P., Vinciguerra, S., 2014. The effects of rock heterogeneity on compaction localization in porous carbonates. J. Struct. Geol. 67 (Part A), 75–93.
Crider, J.G., Peacock, D.C.P., 2004. Initiation of brittle faults in the upper crust: a

review of field observations. J. Struct. Geol. 26, 691–707.
Crider, J.G., Pollard, D.D., 1998. Fault linkage: three-dimensional mechanical interaction between echelon normal faults. J. Geophys. Res. 103, 24373–24391.
Croizé, D., Bjørlykke, K., Jahren, J., Renard, F., 2010. Experimental mechanical and chemical compaction of carbonate sand. J. Geophys. Res. Solid Earth 115 (n/a-n/a).
Dart, C.J., Bosence, D.W.J., McClay, K.R., 1993. Stratigraphy and structure of the Maltese graben system. J. Geol. Soc. 150, 1153–1166.
Deng, S., Zuo, L., Aydin, A., Dvorkin, J., Mukerji, T., 2015. Permeability characterization of natural compaction bands using core flooding experiments and three-dimensional image-based analysis: comparing and contrasting the results from two different methods. AAPG Bull. 99, 27–49.
Du Bernard, X., Eichhubl, P., Aydin, A., 2002. Dilation bands: a new form of localized failure in granular media. Geophys. Res. Lett. 29, 2176–2179.
Dunham, R.J., 1962. Classification of carbonate rocks according to their depositional texture. In: Ham, W.E. (Ed.), Classification of Carbonate Rocks, pp. 108–121.
Eichhubl, P., Hooker, J.N., Laubach, S.E., 2010. Pure and shear-enhanced compaction bands in Aztec Sandstone. J. Struct. Geol. 32, 1873–1886.
Engelder, J.T., 1974. Cataclasis and the generation of fault gouge. GSA Bull. 85, 1515–1522.
Faure Walker, J.P., Roberts, G.P., Cowie, P.A., Papanikolaou, I.D., Sammonds, P.R., Michetti, A.M., Phillips, R.J., 2009. Horizontal strain-rates and throw-rates across breached relay zones, central Italy: implications for the preservation of throw deficits at points of normal fault linkage. J. Struct. Geol. 31, 1145–1160.
Ferreira, T., Rasband, W., 2012. ImageJ User Guide.
Fisher, Q.J., Knipe, R.J., 2001. The permeability of faults within siliciclastic petroleum reservoirs of the North Sea and Norwegian Continental Shelf. Mar. Pet. Geol. 18, 1063–1081.
Fossen, H., Hesthammer, J., 1997. Geometric analysis and scaling relations of deformation bands in porous sandstone. J. Struct. Geol. 19, 1479–1493.
Fossen, H., Rotevatn, A., 2016. Fault linkage and relay structures in extensional settings—A review. Earth-Sci. Rev. 154, 14–28.
Fossen, H., Johansen, T.E.S., Hesthammer, J., Rotevatn, A., 2005. Fault interaction in porous sandstone and implications for reservoir management; examples from southern Utah. AAPG Bull. 89 (12), 1593–1606.
Fossen, H., Schultz, R.A., Shipton, Z.K., Mair, K., 2007. Deformation bands in sandstone - a review. J. Geol. Soc. Lond. 164, 755–769.
Fossen, H., Schultz, R.A., Torabi, A., 2011. Conditions and implications for compaction band formation in the Navajo Sandstone, Utah. J. Struct. Geol. 33, 1477–1490.
Fossen, H., Zuluaga, L.F., Ballas, G., Soliva, R., Rotevatn, A., 2015. Contractional deformation of porous sandstone: insights from the Aztec Sandstone, SE Nevada, USA. J. Struct. Geol. 74, 172–184.
Grasso, M., Reuther, C.D., Baumann, H., Becker, A., 1986. Shallow crustal stress and neotectonic framework of the Malta Platform and the Southeastern Pantelleria Rift (Central Mediterranean). Geol. Romana 25, 191–212.
Ji, Y., Hall, S.A., Baud, P., Wong, T.-f., 2015. Characterization of pore structure and strain localization in Majella limestone by X-ray computed tomography and digital image correlation. Geophys. J. Int. 200, 701–719.
Kattenhorn, S.A., Aydin, A., Pollard, D.D., 2000. Joints at high angles to normal fault strike: an explanation using 3-D numerical models of fault-perturbed stress fields. J. Struct. Geol. 22, 1–23.
Klimczak, C., Soliva, R., Schultz, R.A., Chéry, J., 2011. Sequential growth of deformation bands in a multilayer sequence. J. Geophys. Res. Solid Earth 116 (n/a-n/a).
Liu, C., Pollard, D.D., Deng, S., Aydin, A., 2015. Mechanism of formation of wiggly compaction bands in porous sandstone: 1. observations and conceptual model. J. Geophys. Res. Solid Earth 120 (12), 8138–8152.
Mair, K., Elphick, S., Main, I., 2002. Influence of confining pressure on the mechanical and structural evolution of laboratory deformation bands. Geophys. Res. Lett. 29 http://dx.doi.org/10.1029/2001GL013964.
Mair, K., Main, I., Elphick, S., 2000. Sequential growth of deformation bands in the laboratory. J. Struct. Geol. 22, 25–42.
Mandl, G., DeJong, L.N.J., Maltha, A., 1977. Shear zones in granular material. Rock Mech. 9, 95–144.
Marchegiani, L., Van Dijk, J.P., Gillespie, P.A., Tondi, E., Cello, G., 2006. Scaling properties of the dimensional and spatial characteristics of fault and fracture systems in the Majella Mountain, central Italy. Special Publications 261 Geol. Soc. Lond. 113–131.
Micarelli, L., Benedicto, A., Wibberley, C.A.J., 2006. Structural evolution and permeability of normal fault zones in highly porous carbonate rocks. J. Struct. Geol. 28, 1214–1227.
Michie, E.A.H., 2015. Influence of host lithofacies on fault rock variation in carbonate fault zones: a case study from the Island of Malta. J. Struct. Geol. 76, 61–79.
Michie, E.A.H., Haines, T.J., Healy, D., Neilson, J.E., Timms, N.E., Wibberley, C.A.J., 2014. Influence of carbonate facies on fault zone architecture. J. Struct. Geol. 65, 82–99.
Mollema, P.M., Antonellini, M., 1996. Compaction bands: a structural analog for anti-mode I cracks in aeolian sandstone. Tectonophysics 267, 209–228.
Ohlmacher, G.C., Aydin, A., 1997. Mechanics of vein, fault and solution surface formation in the Appalachian valley and ridge, northeastern tennessee, U.S.A.: implications for fault friction, state of stress and fluid pressure. J. Struct. Geol. 19, 927–944.
Peacock, D.C.P., Fisher, Q.J., Willemse, E.J.M., Aydin, A., 1998. The relationship between faults and pressure solution seams in carbonate rocks and the implications for fluid flow. Special Publications Geol. Soc. Lond. 147, 105–115.
Peacock, D.C.P., Parfitt, E.A., 2002. Active relay ramps and normal fault propagation on Kilauea Volcano, Hawaii. J. Struct. Geol. 24, 729–742.
Pedley, H.M., House, M.R., Waugh, B., 1976. The geology of Malta and Gozo. Proc. Geol. Assoc. 87, 325–341.
Pedley, H.M., 1993. Geological Map of the Islands of Malta, 1:25,000 scale. British Geological Survey, Keyworth, Nottinghamshire, UK.
Putz-Perrier, M.W., Sanderson, D.J., 2010. Distribution of faults and extensional strain in fractured carbonates of the North Malta Graben. AAPG Bull. 94, 435–456.
Rath, A., Exner, U., Tschegg, C., Grasemann, B., Laner, R., Draganits, E., 2011. Diagenetic control of deformation mechanisms in deformation bands in a carbonate grainstone. AAPG Bull. 95, 1369–1381.
Rawling, G.C., Goodwin, L.B., 2003. Cataclasis and particulate flow in faulted, poorly lithified sediments. J. Struct. Geol. 25, 317–331.
Rotevatn, A., Sandve, T.H., Keilegavlen, E., Kolyukhin, D., Fossen, H., 2013. Deformation bands and their impact on fluid flow in sandstone reservoirs: the role of natural thickness variations. Geofluids. 13 (3), 359–371.
Rotevatn, A., Bastesen, E., 2014. Fault linkage and damage zone architecture in tight carbonate rocks in the Suez Rift (Egypt): implications for permeability structure along segmented normal faults. Special Publications Geol. Soc. Lond. 374, 79–95.
Rotevatn, A., Fossen, H., Hesthammer, J., Aas, T.E., Howell, J.A., 2007. Are relay ramps conduits for fluid flow? structural analysis of a relay ramp in Arches National Park, Utah. In: Lonergan, L., Jolly, R.J.H., Sanderson, D.J., Rawnsley, K. (Eds.), Fractured Reservoirs. Geological Society, London, pp. 55–71. Special Publications.
Rotevatn, A., Torabi, A., Fossen, H., Braathen, A., 2008. Slipped deformation bands: a new type of cataclastic deformation bands in Western Sinai, Suez rift, Egypt. J. Struct. Geol. 30, 1317–1331.
Rustichelli, A., Tondi, E., Agosta, F., Cilona, A., Giorgioni, M., 2012. Development and distribution of bed-parallel compaction bands and pressure solution seams in carbonates (Bolognano Formation, Majella Mountain, Italy). J. Struct. Geol. 37, 181–199.
Schultz, R.A., Okubo, C.H., Fossen, H., 2010. Porosity and grain size controls on compaction band formation in Jurassic Navajo Sandstone. Geophys. Res. Lett. 37 (n/a-n/a).
Sternlof, K.R., Chapin, J.R., Pollard, D.D., Durlofsky, L.J., 2004. Permeability effects of deformation band arrays in sandstone. AAPG Bull. 88, 1315–1329.
Sylvester, A.G., 1988. Strike-slip faults. Geol. Soc. Am. Bull. 100, 1666–1703.
Taylor, A.M., Goldring, R., 1993. Description and analysis of bioturbation and ichnofabric. J. Geol. Soc. 150, 141–148.
Taylor, W.L., Pollard, D.D., 2000. Estimation of in-situ permeability of deformation bands in porous sandstone, Valley of Fire, Nevada. Water Resour. Res. 36, 2595–2606.
Tondi, E., 2007. Nucleation, development and petrophysical properties of faults in carbonate grainstones: evidence from the San Vito Lo Capo peninsula (Sicily, Italy). J. Struct. Geol. 29, 614–628.
Tondi, E., Antonellini, M., Aydin, A., Marchegiani, L., Cello, G., 2006. The role of deformation bands, stylolites and sheared stylolites in fault development in carbonate grainstones of Majella Mountain, Italy. J. Struct. Geol. 28, 376–391.
Tondi, E., Cilona, A., Agosta, F., Aydin, A., Rustichelli, A., Renda, P., Giunta, G., 2012. Growth processes, dimensional parameters and scaling relationships of two conjugate sets of compactive shear bands in porous carbonate grainstones, Favignana Island, Italy. J. Struct. Geol. 37, 53–64.
Tondi, E., Rustichelli, A., Cilona, A., Balsamo, F., Storti, F., Napoli, G., Agosta, F., Renda, P., Giorgioni, M., 2016. Hydraulic properties of fault zones in porous carbonates, examples from central and southern Italy. Ital. J. Geosci. 135, 68–79.
Torabi, A., Fossen, H., 2009. Spatial variation of microstructure and petrophysical properties along deformation bands in reservoir sandstones. AAPG Bull. 93 (7), 919–938.
Torabi, A., Aydin, A., Cilona, A., Jarstø, B.E., Deng, S., 2015. The dynamics and interaction of compaction bands in Valley of Fire State Park, Nevada (USA): implications for their growth, evolution, and geostatistical property. Tectonophysics 657, 113–128.
Vajdova, V., Baud, P., Wong, T.-f., 2004. Compaction, dilatancy, and failure in porous carbonate rocks. J. Geophys. Res. Solid Earth 109 (n/a-n/a).
Vajdova, V., Baud, P., Wu, L., Wong, T.-f., 2012. Micromechanics of inelastic compaction in two allochemical limestones. J. Struct. Geol. 43, 100–117.
Vajdova, V., Zhu, W., Natalie Chen, T.-M., Wong, T.-f., 2010. Micromechanics of brittle faulting and cataclastic flow in Tavel limestone. J. Struct. Geol. 32, 1158–1169.
Wennberg, O.P., Casini, G., Jahanpanah, A., Lapponi, F., Ineson, J., Wall, B.G., Gillespie, P., 2013. Deformation bands in chalk, examples from the Shetland group of the Oseberg Field, North Sea, Norway. J. Struct. Geol. 56, 103–117.
Willemse, E.J.M., Peacock, D.C.P., Aydin, A., 1997. Nucleation and growth of strike-slip faults in limestones from Somerset, U.K. J. Struct. Geol. 19, 1461–1477.
Wong, T.-F., 1990. Mechanical compaction and the brittle—ductile transition in porous sandstones. Special Publications Geol. Soc. Lond. 54, 111–122.
Zhu, W., Baud, P., Wong, T.-f., 2010. Micromechanics of cataclastic pore collapse in limestone. J. Geophys. Res. Solid Earth 115, B04405 doi:04410.01029/02009JB006610.